NACA

RESEARCH MEMORANDUM

COMPARISON OF SEMISPAN AND FULL-SPAN TESTS OF A 47.5° SWEPTBACK WING WITH SYMMETRICAL CIRCULAR-ARC SECTIONS AND HAVING DROOPED-NOSE FLAPS, TRAILING-EDGE FLAPS, AND AILERONS

By Stanley Lipson and U. Reed Barnett, Jr.

Langley Aeronautical Laboratory
Langley Field, Va.

NATIONAL ADVISORY COMMITTEE
FOR AERONAUTICS

WASHINGTON
December 5, 1951

NACA RM L51H15

NATIONAL ADVISORY COMMITTEE FOR AERONAUTICS

RESEARCH MEMORANDUM

COMPARISON OF SEMISPAN AND FULL-SPAN TESTS OF A 47.5° SWEPTBACK WING WITH SYMMETRICAL CIRCULAR-ARC SECTIONS AND HAVING DROOPED-NOSE FLAPS, TRAILING-EDGE FLAPS, AND AILERONS

By Stanley Lipson and U. Reed Barnett, Jr.

SUMMARY

In order to help evaluate the general validity of the semispan wing testing technique in the Langley full-scale tunnel, an investigation was conducted to compare the characteristics of a full-span and a semispan highly swept wing. Wing surface pressure and force measurements were obtained on a semispan model of a 47.5° sweptback wing for which full-span data were available. The wing had symmetrical biconvex airfoil sections 10 percent thick and had an aspect ratio of 3.5, a taper ratio of 0.5, and no geometric dihedral or twist. The configurations investigated included the basic wing, the wing with a drooped-nose flap and a trailing-edge flap deflected both alone and in combination, and the basic wing with a deflected aileron. The data were obtained at a Reynolds number of 4.2×10^6 and a Mach number of 0.07.

The results indicate close agreement between the full-span- and semispan-wing data and demonstrate the acceptability of the semispan method of testing for wings similar to the one investigated. Slightly higher maximum lift coefficients at a higher angle of attack and a more negative pitching tendency over a large part of the lift range were observed for the semispan wing. These differences in the wing characteristics are believed to be due to a loss of lift near the root of the semispan wing and to a shift of the leading-edge separation-vortex origin from the wing apex caused by the interference of the reflection-plane boundary layer.

INTRODUCTION

An evaluation of the future wing research program of the Langley full-scale tunnel indicated that, for many of the planned wing

configurations, it would be advantageous to use a semispan testing arrangement. The semispan system permits the use of larger models; thus, the available Reynolds number range is increased. In addition the semispan system facilitates the use of special equipment required for various types of boundary-layer control applications.

Previous investigations to determine the correlation between full-span and semispan wing tests have been conducted and are reported in references 1, 2, and 3. In order to obtain information on a more highly swept wing than those previously investigated and, in addition, to determine the adequacy of the reflection-plane arrangement in the Langley full-scale tunnel, tests were conducted on a wing panel of a 47.5° sweptback wing. This wing has been extensively tested in the full-span configuration in the Langley full-scale tunnel (references 4, 5, and 6). The investigation was conducted at a Reynolds number of 4.2×10^6 and a Mach number of 0.07. The aerodynamic force and moment characteristics and the wing surface-pressure distribution were obtained over a large angle-of-attack range. The longitudinal characteristics of the basic wing and the wing with drooped-nose and plain trailing-edge flaps were investigated and, in addition, the rolling-moment characteristics for the basic wing with a 0.50 semispan aileron deflected were also obtained.

COEFFICIENTS AND SYMBOLS

The test data are presented as standard NACA coefficients of forces and moments. The data are referred to a set of axes coinciding with the wind axes, and the origin is located at the quarter-chord point of the mean aerodynamic chord. Lift, drag, and pitching moment represent full-span values or twice semispan values.

Force coefficients:

C_L lift coefficient $\left(\frac{\text{Lift}}{q_o S}\right)$

$C_{L_{max}}$ maximum lift coefficient

C_D drag coefficient $\left(\frac{\text{Drag}}{q_o S}\right)$

C_m pitching-moment coefficient about the quarter-chord point of the mean aerodynamic chord $\left(\frac{\text{Pitching moment}}{q_o S \bar{c}}\right)$

C_{l_u} uncorrected rolling-moment coefficient, measured in semispan wing tests $\left(\frac{\text{Rolling moment}}{q_o S b}\right)$

C_l corrected rolling-moment coefficient, measured in full-span tests and for semispan tests $\left(C_l = C_{l_u} - 2\Delta C_{l_r}\right)$

C_{l_a} corrected rolling-moment coefficient due to aileron deflection

ΔC_{l_r} one-half rolling-moment-coefficient correction due to reflection plane

Pressure coefficients:

C_L' approximate lift coefficient $\left(\int_0^1 c_l' \frac{c}{c_{av}} d\left(\frac{2y}{b}\right)\right)$

C_m' pitching-moment coefficient about the quarter-chord point of the mean aerodynamic chord

$$\left(\frac{c_{av}}{\bar{c}} \int_0^1 \frac{c_n}{c}(\bar{x}') \left(\frac{c}{c_{av}}\right)^2 d\left(\frac{2y}{b}\right)\right)$$

c_l' approximate section lift coefficient $\left(\cos \alpha \int_0^1 P_r \, d\left(\frac{x}{c}\right)\right)$

c_n section normal-force coefficient $\left(\int_0^1 P_r \, d\left(\frac{x}{c}\right)\right)$

$c_{l_b}' \frac{c}{c_{av}}$ basic load coefficient, local wing loading at zero lift

$c_{l_a}' \frac{c}{c_{av}}$ additional load coefficient

$P_r = P_{\text{lower surface}} - P_{\text{upper surface}}$

P pressure coefficient $\left(\frac{p - p_o}{q_o}\right)$

Symbols:

$\bar{x}'$ longitudinal distance from local center of pressure to quarter-chord point of the mean aerodynamic chord, feet

p local static pressure, pounds per square foot

q local dynamic pressure, pounds per square foot

p_o free-stream static pressure, pounds per square foot

q_o free-stream dynamic pressure, pounds per square foot

c.p. chordwise section center of pressure, percent chord

x chordwise coordinate parallel to plane of symmetry, feet

y spanwise coordinate perpendicular to plane of symmetry, feet

b wing span, feet

c local chord measured parallel to plane of symmetry, feet

c' local chord measured perpendicular to line of maximum thickness (0.50c'), feet

$\bar{c}$ mean aerodynamic chord, feet $\left(\frac{2}{S}\int_0^{b/2} c^2 dy\right)$

c_{av} average chord, feet (S/b)

S wing area, (twice area of semispan wing) square feet

α angle of attack, degrees

$\alpha_{C_{L_{max}}}$ angle of attack for wing maximum lift coefficient, degrees

$\alpha_{c_l', max}$ angle of attack for section maximum lift coefficient, degrees

δ_a aileron-deflection angle, degrees

TESTING ARRANGEMENT

Reflection Plane

The reflection plane as installed in the Langley full-scale tunnel is shown in figure 1. The plane is 52 feet long and 42.5 feet wide. The surface of the plane is smooth and is leveled to a tolerance of ±1/16 inch. The vertical location of the plane is about 18 inches above the lower lip of the wind-tunnel entrance cone and projects approximately 2.5 feet upstream of the entrance cone lip. The leading edge of the reflection plane is semicircular in cross section.

A 14-foot-diameter turntable rotates with the semispan wing models during angle-of-attack changes and the center of the turntable is on the tunnel's longitudinal axis, 19.5 feet from the leading edge of the reflection plane. This location places the semispan models in approximately the same longitudinal tunnel location as that at which the full-span models are tested. The general arrangement for the semispan wing tests is illustrated by figure 2.

When force data are being obtained, the semispan model is completely independent of the force acting upon the turntable. Various types of seals were tested for use at the cut-out in the turntable through which the semispan wing projects. The configuration adopted consisted of a strip of felt glued to the surface of the wing and a soft rubber strip, which was attached to the turntable and "feathered" against the felt. Flow surveys indicated that this seal minimized the flow leakage through the turntable cut-out and force measurements showed that the seal had only a negligible effect.

Model

The wing was swept back 47.5° at the leading edge and had an aspect ratio of 3.5, a taper ratio of 0.5, and no geometric dihedral or twist. The airfoil section perpendicular to the 0.50c' line was a 0.10c'-thick symmetrical circular-arc section. Figure 3 shows the wing plan form and presents some of the more pertinent dimensions. A detailed description of the wing construction is given in reference 4.

[redacted]

The flaps, which are described fully in reference 5, were 0.20c' plain flaps. When the flaps, which are hinged at the lower surface, were deflected, the resulting gaps on the upper wing surface were covered and faired by means of sheet-metal seals. The flap-deflection angles were measured perpendicular to the hinge line. The aileron configuration employed consisted of deflecting the outboard $0.50\frac{b}{2}$ section of the trailing-edge flap.

Flush surface static-pressure orifices were installed in the wing in chordwise rows (streamwise direction) at 5, 10, 20, 40, 60, and 80 percent of the wing semispan. The general arrangement of the orifices on the wing and their chordwise locations are presented in figure 4.

Flow Conditions

In order to determine the flow conditions at and directly above the surface of the reflection plane, tuft and pressure surveys were conducted. The wool-strand tufts were attached both to the surface of the plane and to masts to give a rapid visualization of the reflection-plane flow conditions. Velocity distributions in the boundary layer were obtained by means of rakes, which are shown mounted on the reflection plane in figure 2. The data obtained in the boundary-layer surveys at the two stations most representative of the semispan wing location are presented in figure 5 and agree qualitatively with the results of the tuft surveys, which showed no indication of local separation on the reflection plane in the area of interest around the model location. Although the boundary-layer total thickness at the station 19.5 feet behind the leading edge of the reflection plane (the location of the center of the turntable) is appreciable, approximately 5.5 inches, it represents only slightly more than 3 percent of the 14.25-foot span of the semispan model. In reference 1 a boundary-layer total thickness of approximately 5 percent of the wing semispan was found acceptable for most test conditions of a 40° sweptback wing. Data presented in reference 1 also showed, however, that, for certain "sensitive" flapped configurations the wing characteristics may be severely altered because of the effects of this boundary-layer condition on the flow at the inboard section of the wing.

The results obtained with a former reflection-plane arrangement in the Langley full-scale tunnel are reported in reference 3. The boundary-layer total thickness due to that reflection-plane installation also was about 5 inches at the model location whereas, above that height, the tunnel dynamic-pressure distribution varied a maximum of $0.012q_o$ and $-0.018q_o$ from the mean value. From that very complete dynamic-pressure survey and from recent tunnel-flow measurements with the present

[redacted]

reflection plane installed, it is believed that, above the boundary-layer thickness, the variation in stream dynamic pressure obtained along the span of the semispan models is no greater than that existing for the full-span wings tested in the normal horizontal position.

TESTS AND CORRECTIONS

Tests

The semispan results reported herein were obtained on separate wing panels since the angle-of-attack drive system for the semispan balance-testing arrangement was designed for left wing panels, and only the right wing panel of the 47.5° sweptback wing was equipped with orifice tubes; thus a separate setup was required.

Pressure tests.- The semispan-wing surface-pressure investigation included five configurations: (1) basic wing; (2) wing with $1.00\frac{b}{2}$ drooped-nose flap deflected 40°; (3) wing with $0.50\frac{b}{2}$ trailing-edge flap deflected 40°; (4) combination of configurations (2) and (3); and (5) basic wing with the $0.50\frac{b}{2}$ aileron deflected 19.6°. These configurations and the angle-of-attack range were chosen so as to duplicate those of the previous full-span wing investigation.

Force tests.- The force measurements on the semispan wing were obtained over an angle-of-attack range of approximately -2° to 31° and covered five configurations for which comparative full-span force data were available: (1) basic wing; (2) wing with $1.00\frac{b}{2}$ drooped-nose flap deflected 30°; (3) wing with $1.00\frac{b}{2}$ trailing-edge flap deflected 40°; (4) combination of configurations (2) and (3); and (5) basic wing with the $0.50\frac{b}{2}$ aileron deflected.

The pressure and force data were obtained at a Reynolds number of 4.2×10^6 and at a Mach number of 0.07.

Method of Corrections

The jet-boundary corrections applied to the data were computed by the method discussed in reference 7. The induced downwash effects along the span of the wing were determined from chart contours giving the jet-boundary induced velocities normal to the wing. The theoretical

basis for the charts is discussed fully in reference 8 which, in addition, illustrates one of the charts used for the downwash calculations in the Langley full-scale tunnel.

Reference 7 points out that the complete angle-of-attack correction (jet-boundary plus stream curvature) is equivalent to the induced downwash angle along the three-quarter-chord line.

$$\Delta\alpha = -1.96C_L \text{(Full-span wing)}$$

$$\Delta\alpha = -0.64C_L \text{(Semispan wing)}$$

The correction to the drag coefficient is based on the tunnel-induced downwash at the quarter-chord line.

$$\Delta C_D = -0.02835C_L^2 \text{(Full-span wing)}$$

$$\Delta C_D = -0.00938C_L^2 \text{(Semispan wing)}$$

The tunnel-induced increment in pitching moment is produced by two induced lift effects: first, the lift increment at the quarter-chord line of the wing resulting from the induced downwash; secondly, as more fully discussed in reference 7, the lift increment due to the induced camber effect, a result of the angular differential between the induced downwash angles at the quarter- and three-quarter-chord lines.

$$\Delta C_m = -0.02001C_L \text{(Full-span wing)}$$

$$\Delta C_m = -0.00526C_L \text{(Semispan wing)}$$

All corrections are added to the uncorrected data. The data presented herein have also been corrected for the effects of blockage, stream angle, and for the strut tares of the full-span wing tests.

The correction to be applied to the rolling moment is composed of two parts: the effect of the image wing on the span-load distribution and the change in the jet-boundary corrections resulting from the deflection of the aileron.

The semispan-wing rolling-moment coefficients due to aileron deflection were modified for the reflection-loading effect by the methods discussed in reference 9. The correction factor to be applied to the measured rolling-moment coefficients for the semispan wing $1 + \frac{2\Delta C_{l_r}}{C_l}$

was obtained from unpublished charts based on the modified Weissinger method presented in reference 10. Computations of the rolling-moment-coefficient correction due to the jet-boundary effects induced by deflecting the aileron were made for the largest aileron deflection. As the resultant increment was small in relationship to the rolling-moment coefficient due to the aileron deflection, no calculations were performed for the other deflection angles, nor was the computed increment for the largest deflection angle applied to the data.

PRESENTATION OF DATA

The results of the tests are presented as discussions of lift, drag, pitching-moment, and rolling-moment characteristics. In order to facilitate the analysis and discussion of the lift and pitching-moment characteristics, chordwise pressure-distribution plots are given (figs. 6 to 9) to show comparative full-span and semispan pressure distributions at approximately equal angles of attack.

The lift data obtained from the pressure tests are presented in figures 10 to 18 and the lift coefficients from the force data are shown in figure 19. The drag coefficients are derived from the force data only and are also given in figure 19. The pitching-moment data obtained from the pressure measurements are presented in figures 10 and 15 and from the force data in figure 20. The location of the spanwise wing center of pressures, from both pressure and force data is given in figure 21, and the variation of dC_m/dC_L with lift coefficient in figure 22. Data for the aileron deflected configuration derived from the force measurements are presented in figure 23 and those derived from the pressure data are given in figures 24 and 25. Figure 26 compares the spanwise center of pressure computed from both the force and pressure data for the wing with the aileron deflected 19.6°.

DISCUSSION

A preliminary analysis of the data indicates the strong influence of the leading-edge separation vortex on the comparison of the semispan and full-span wing characteristics. (For a detailed description of the characteristics and the effects of the vortex flow over the full-span wing, see reference 6.) As the presence and strength of the vortex are dependent upon many variables such as angle of sweep, wing thickness, and leading-edge configuration, it is not considered advisable to use the analysis of one wing plan form as a basis for determining any all-inclusive correlation between full-span- and semispan-wing results.

[redacted]

The results discussed, however, are believed to be of value to demonstrate, at large scale, the change in comparative wing characteristics between full-span- and semispan-wing tests when separation-vortex-type wing flow is present.

Lift Characteristics

The lift characteristics (fig. 19) show close agreement between the full-span- and semispan-wing data throughout the angle-of-attack range for all configurations tested. The data, however, show slightly higher values of $C_{L_{max}}$ and $\alpha_{C_{L_{max}}}$ for the semispan wing than for the full-span wing for all configurations. Below $C_{L_{max}}$ and especially in the moderate C_L range, the semispan wing had lower values of C_L, about 0.03, than did the full-span wing. The same effect is indicated by the pressure data for the basic wing configuration (fig. 15). Comparable results were also obtained in a similar investigation comparing the characteristics of a full span and semispan 40° sweptback wing (reference 1).

Although the agreement in lift values for the full-span and semispan wings is comparatively close, it is believed to be of general interest to discuss the flow changes that cause the small differences in the lift characteristics but that effect even larger differences in the pitching-moment characteristics. Figure 14 shows a loss in additional loading at the inboard stations of the semispan wing which continues to increase with increasing α in contrast to the effect of α on the additional loading comparison for the outboard sections of the wing. This decrease in lift effectiveness at the stations inboard of $0.10\frac{b}{2}$ is believed to be an effect characteristic of the results obtained with semispan wings mounted on reflection planes. Previous tests of a moderately sweptback wing tested semispan and full span (reference 2) also showed a loss in the additional-load parameter for the semispan wing over the inboard 10 percent of the wing semispan. Similar results have been obtained with unswept semispan wings, as indicated by reference 3.

A study of the chordwise pressure distributions for the basic wing (fig. 6) reveals that the "hump" in the chordwise pressure distributions, which characterizes the vortex-type flow, is usually broader and slightly farther rearward for the full-span wing. This change in flow characteristics is believed to be due to a shift of the vortex origin outboard from the wing apex caused by the interference of the reflection-plane boundary layer. During the investigation reported in reference 1, indications were obtained of a flow change due to the tunnel-wall

boundary layer (semispan model was cantilevered through the tunnel wall) which resulted in a delay in the separation of the flow from the root of the semispan wing.

Observations of wool-strand tufts attached to the upper surface of the full-span and semispan wing also indicated this shift in the vortex origin. The flow effects of the separation vortex on the semispan wing were markedly similar to those observed for the full-span wing but consistently occurred at higher angles of attack. The tuft surveys indicated that, at the same angle of attack, the origin of the leading-edge spanwise flow was always more outboard for the semispan wing than for the full-span wing. This flow difference was noted until the angle of attack for maximum lift was reached.

The result of this more outboard location of the vortex origin is effectively to delay the development of the vortex at any station on the semispan wing and thus give a higher $\alpha_{c_{l'_{max}}}$ as compared with the value obtained at the corresponding station on the full-span wing. At the three most outboard stations $\left(0.40, 0.60, \text{and } 0.80\frac{b}{2}\right)$ in the angle-of-attack range below $\alpha_{c_{l'_{max}}}$, the result of delaying the vortex formation is a smaller increase in section lift coefficient for the semispan wing (fig. 10). Past $\alpha_{c_{l'_{max}}}$, however, the section lift characteristics for the semispan wing at the $0.40\frac{b}{2}$ and $0.60\frac{b}{2}$ stations exhibit a marked increase in effectiveness over the results obtained for the full-span wing.

It appears, then, that in the moderate angle-of-attack range the loss of lift near the wing root, due to reflection plane effects, and the loss of lift due to the less effective vortex action at the outboard stations which are at an angle of attack below $\alpha_{c_{l'_{max}}}$ combine to lower the total lift of the semispan wing as compared with the full-span configuration. When the wing angle of attack is increased to a value greater than the $\alpha_{c_{l'_{max}}}$ for a large part of the wing, then the previously discussed increased effectiveness of the semispan-wing chordwise sections operating beyond $\alpha_{c_{l'_{max}}}$ tends to counteract the aforementioned lift losses. Finally, at the higher angles of attack the total lift of the semispan wing exceeds that measured for the full-span wing.

With the drooped-nose flap deflected (fig. 19(b)) the wing lift curve is essentially linear between $\alpha = 7^\circ$ and $\alpha = 18^\circ$ and shows no

indication of the presence of the vortex-type flow. In this α range there is an appreciable increase in C_L for the full-span wing over that obtained with the semispan wing which is probably due, as previously discussed, to the inboard loss of lift resulting from the reflection-plane effects. At an angle of attack of approximately 18°, however, both the section lift curves for the outer wing sections (fig. 11) and the wing lift curve (fig. 19(b)) indicate that the vortex has appeared on the wing upper surface. For angles of attack greater than 18°, the comparative lift characteristics of the semispan and full-span wings, with the drooped-nose flap deflected, resemble the results obtained from the basic wing tests in that the flow effects due to the outboard shift in the origin of the vortex on the semispan wing compensate for the inboard loss of lift.

With the trailing-edge flap deflected, a comparison of the pressure-data lift values C_L' for the full-span and semispan wings (fig. 17) does not show the close agreement obtained from the comparison of the force-data lift coefficients (fig. 19(c)). This disagreement can be traced to the increased section lift coefficients indicated by the pressure data at sections $0.10\frac{b}{2}$ and $0.20\frac{b}{2}$ (fig. 12) for the semispan wing with the semispan trailing-edge flap deflected. The reason for this increased effectiveness is not evident from the available data.

For the wing with both the full-span drooped-nose flap and the trailing-edge flap deflected, the lift results measured for the full-span and semispan wings compare in a manner very similar to that obtained with the drooped-nose flap deflected alone. The pressure data for this configuration, when compared either as section or wing lift coefficients, show that there is good agreement between the semispan and full-span wing results.

Drag Characteristics

The drag coefficient data obtained with the semispan wing is, in general, in good agreement with the full-span wing results (fig. 19). With the drooped-nose flap deflected alone, however, the drag coefficients measured for the semispan wing in the moderate lift-coefficient range are greater by about $C_D = 0.004$ than those obtained with the full-span wing at comparable lift coefficients. This disagreement in the moderate C_L range may be due to a change in the flow at the wing tip caused by the difference of 0.7° in angle of attack between the two wing configurations when the comparison is based on constant lift coefficient. (See fig. 19(b).)

During the semispan-wing investigation the sheet-metal fairing used at the juncture of the deflected trailing-edge flap with the wing upper surface at the flap hinge line was somewhat smoother than that employed during the full-span wing tests (reference 5). This difference in fairings may be the source of the slightly lower drag coefficients shown for the semispan wing in the low lift-coefficient range for the tests with the trailing-edge flap deflected (figs. 19(c) and 19(d)).

Pitching-moment Characteristics

The comparative pitching-moment characteristics of the full-span and semispan wings, as obtained from force data, are presented in figure 20. In the low and moderate lift range the semispan wing pitching-moment coefficients are consistently more negative than those measured for the full-span wing. This negative trim shift was also obtained in the semispan tests of references 1 and 3.

For the tests reported herein, with flaps undeflected or with the full-span trailing-edge flaps deflected alone, this negative increment in pitching-moment coefficient increased as lift coefficient increased up to the lift-coefficient value at which the pitching-moment curves break unstable. With the drooped-nose flap deflected, however, the pitching-moment-coefficient difference between the full-span and semispan wing tests decreases with increasing lift coefficient. A comparison of the semispan- and full-span-wing pitching-moment data of reference 1 showed a similar effect when an extensible leading-edge flap was deflected.

The change in flow conditions that produces the difference between the longitudinal stability of the full-span and semispan wings is not too evident from the wing-surface pressure data. Since the basic wing chordwise loadings show practically no chordwise shift in local center of pressure between the full-span and semispan wing tests, it would appear that the negative C_m shift obtained in the semispan-wing tests in the low and moderate C_L range is due almost entirely to an outboard movement in the wing center of pressure. The probable reason for this center-of-pressure shift is the aforementioned characteristic reduction in lift near the wing root for semispan wings mounted on reflection planes. Reference 2, however, shows not only a loss in lift inboard for the semispan wing but also a large rearward shift, further contributing to a more negative pitching moment, in the chordwise center of pressure at a station $0.017\frac{b}{2}$ outboard from the wing root. Integrations of the semispan-wing spanwise loadings obtained from the pressure data, even when modified for the assumption that the root section carried no load because of the reflection-plane boundary layer indicate a more inboard wing center of pressure than that measured during the full-span wing pressure-distribution tests (fig. 21). The

[redacted]

spanwise position of the wing center of pressure as determined from the semispan force data, however, reveals a far more outboard location than that indicated by the pressure tests. This discrepancy between the semispan wing force and pressure results may be due to an insufficient number of chordwise pressure-measuring stations along the span.

The variation of dC_m/dC_L with lift coefficient is presented in figure 22 and, as shown, the curves for the full-span- and semispan-wing tests agree fairly well as to the general magnitudes of the dC_m/dC_L values and to the lift coefficients where the stability changes occur. As indicated from the variation of C_m with C_L, the agreement of the dC_m/dC_L curves are improved with the deflection of the full-span drooped-nose flap.

Rolling-moment characteristics.- A comparison of the full-span- and semispan-wing rolling-moment coefficients due to aileron deflection is presented in figure 23. Although the excellent agreement shown in figure 23 for the basic wing might appear to be fortuitous, because of the difference in the flow characteristics which exists between the full-span and semispan wings, the magnitude of the change in the rolling-moment coefficients that might be attributable to this flow difference would probably be small enough as to be masked by the slight scatter of the C_l data.

The results of the wing surface pressure measurements obtained on the semispan wing with the aileron deflected 19.6° are presented in figures 24, 25, and 26. It should be noted that these pressure data, as well as the spanwise center-of-pressure measurements obtained from the force results (fig. 26), contain the additional loading increment contributed by the reflected aileron deflection.

The effect of the aileron on the loading over the inboard part of the wing is significant but does not appear to vary consistently with a change in angle of attack (fig. 24). The outboard stations indicate a decrease in effectiveness at the higher angles of attack but continue to show a sizeable lift increment due to aileron deflection at the highest test angle of attack (21.2°). The span-loading curves (fig. 25) show that the characteristic type of loading for a wing with a deflected flap-type-control surface was obtained at the lower angles of attack but the shape of the loading curve changes significantly between values of α of 9.4° and 15.3°. The principal cause of this change in loading is the loss of lift over the outboard section of the basic wing in the higher α range (See section on "Lift Characteristics.") rather than the reduction in the section-lift increment induced by the aileron (fig. 24).

[redacted]

The change in span loading at the higher values of α is, of course, reflected in the movement inboard of the spanwise center of pressure which is presented in figure 26. The spanwise centers of pressure as determined from the force and pressure measurements compare exceptionally well. This excellent agreement is in direct contrast with the results obtained in a similar comparison for the basic wing tests (fig. 21).

CONCLUDING REMARKS

An investigation has been conducted in which wing surface pressure measurements and force data were obtained from comparative full-span and semispan tests of a wing having 47.5° of sweepback at the leading edge and an aspect ratio of 3.5. The results indicate close agreement between the full-span- and semispan-wing data and demonstrate the acceptability of the semispan method of testing for wings similar to the one investigated. Slightly higher maximum lift coefficients at a higher angle of attack and a more negative pitching tendency over a large part of the lift range were observed for the semispan wing. These differences in the wing characteristics are believed to be due to a loss of lift near the root of the semispan wing and to a shift of the leading-edge separation-vortex origin from the wing apex caused by the interference of the reflection-plane boundary layer.

Langley Aeronautical Laboratory
National Advisory Committee for Aeronautics
Langley Field, Va.

[redacted]

REFERENCES

1. Cahill, Jones F.: Comparison of Semispan Data Obtained in the Langley Two-Dimensional Low-Turbulence Pressure Tunnel and Full-Span Data Obtained in the Langley 19-Foot Pressure Tunnel for a Wing with 40° Sweepback of the 0.27-Chord Line. NACA RM L9B25a, 1949.

2. Mendelsohn, Robert A., and Brewer, Jack D.: Comparison between the Measured and Theoretical Span Loadings on a Moderately Swept-Forward and a Moderately Swept-Back Semispan Wing. NACA TN 1351, 1947.

3. Parsons, John F., and Silverstein, Abe: Full-Scale Span Load Distribution on a Tapered Wing with Split Flaps of Various Spans. NACA TN 591, 1937.

4. Proterra, Anthony J.: Aerodynamic Characteristics of a 45° Swept-Back Wing with Aspect Ratio of 3.5 and NACA 2S-50(05)-50(05) Airfoil Sections. NACA RM L7C11, 1947.

5. Guryansky, Eugene R., and Lipson, Stanley: Effect of High-Lift Devices on the Longitudinal and Lateral Characteristics of a 45° Sweptback Wing with Symmetrical Circular-Arc Sections. NACA RM L8D06, 1948.

6. Lange, Roy H., Whittle, Edward F., Jr., and Fink, Marvin P.: Investigation at Large Scale of the Pressure Distribution and Flow Phenomena over a Wing with the Leading Edge Swept Back 47.5° Having Circular-Arc Airfoil Sections and Equipped with Drooped-Nose and Plain Flaps. NACA RM L9G15, 1949.

7. Sivells, James C., and Salmi, Rachel M.: Jet-Boundary Corrections for Complete and Semispan Swept Wings in Closed Circular Wind Tunnels. NACA TN 2454, 1951.

8. Katzoff, S., and Hannah, Margery E.: Calculation of Tunnel-Induced Upwash Velocities for Swept and Yawed Wings. NACA TN 1748, 1948.

9. Swanson, Robert S., and Toll, Thomas A.: Jet-Boundary Corrections for Reflection-Plane Models in Rectangular Wind Tunnels. NACA Rep. 770, 1943. (Formerly NACA ARR 3E22.)

10. DeYoung, John: Theoretical Antisymmetric Span Loading for Wings of Arbitrary Plan Form at Subsonic Speeds. NACA TN 2140, 1950.

[redacted]

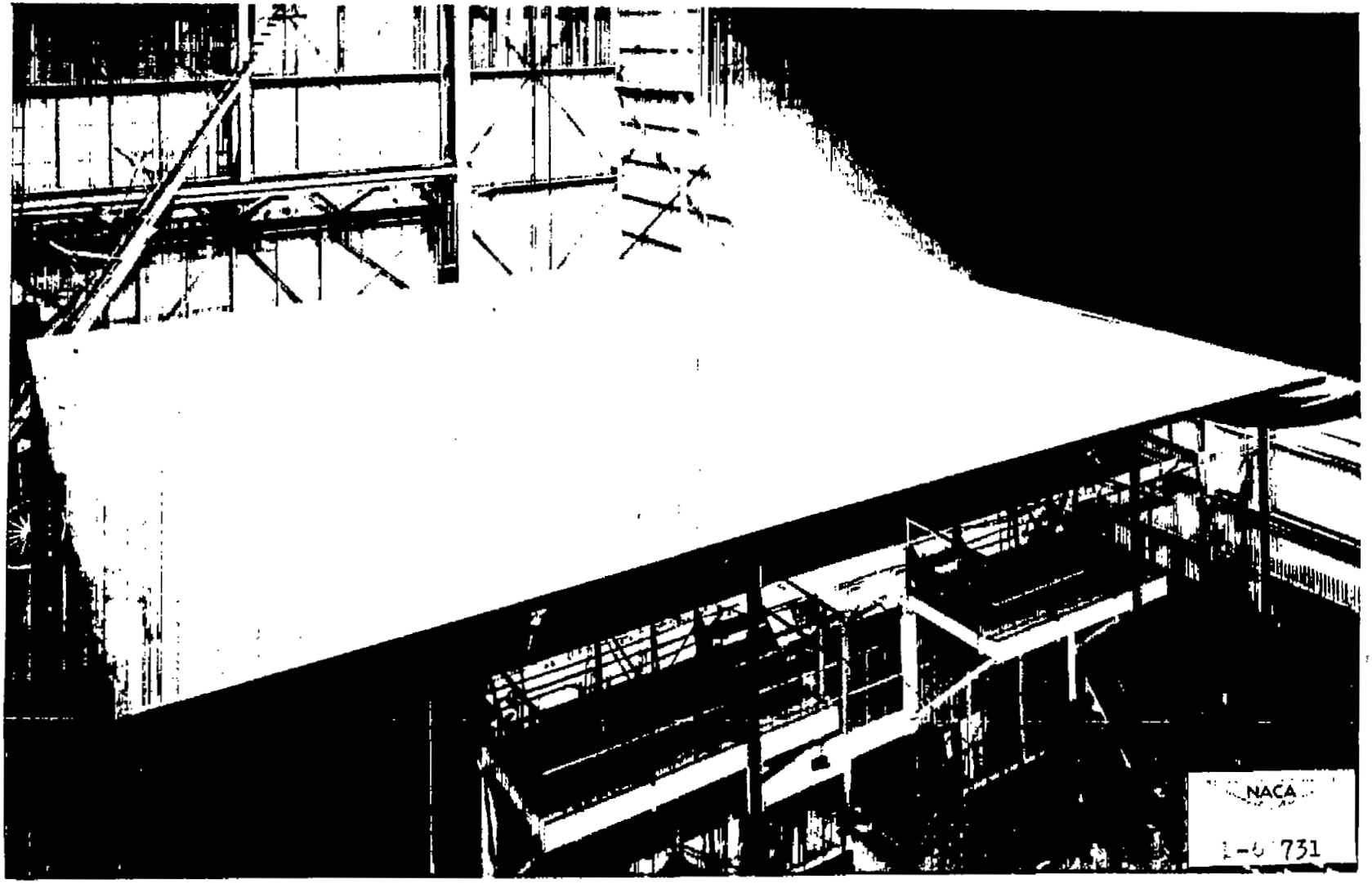

Figure 1.- The reflection plane installed in the Langley full-scale tunnel.

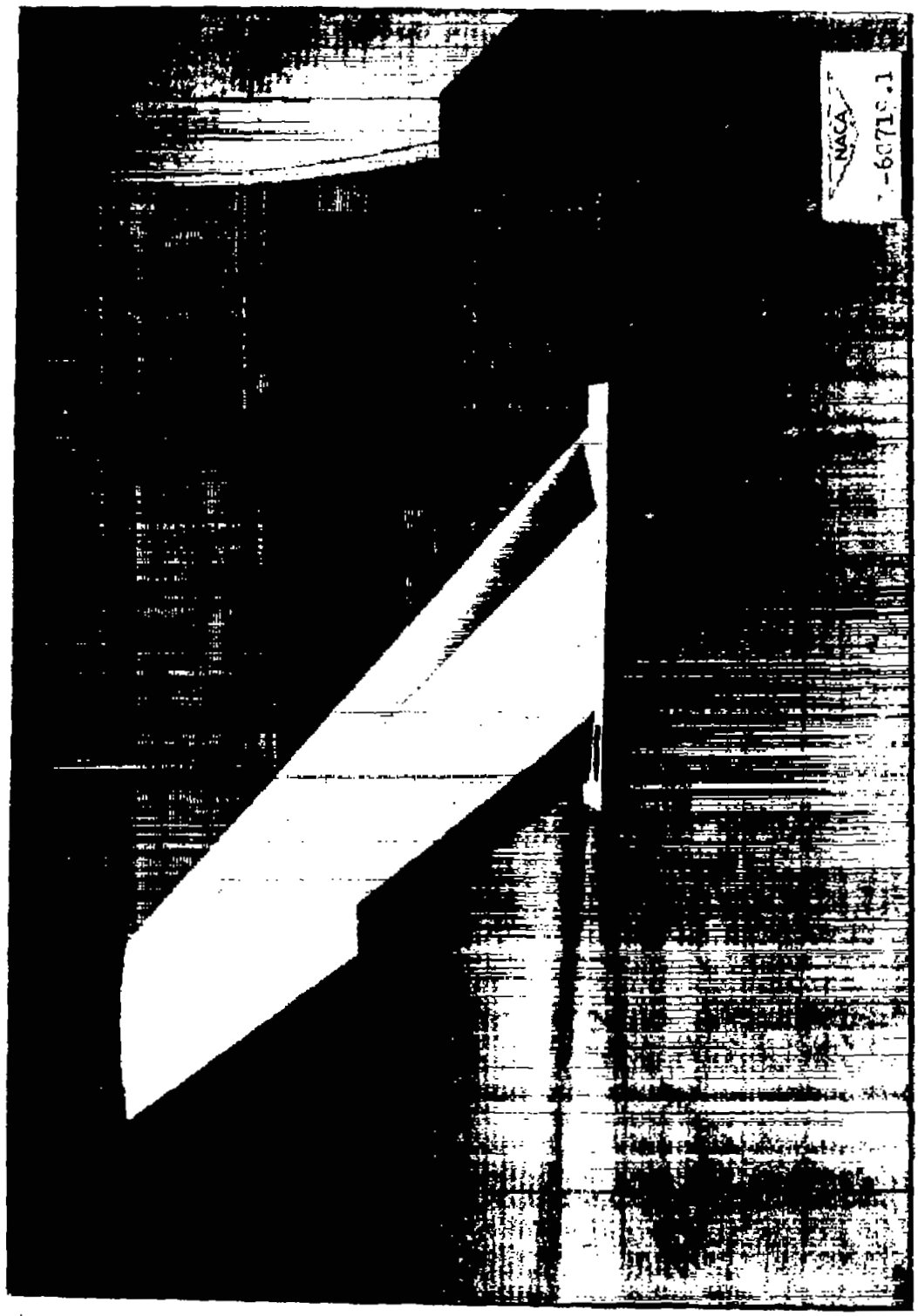

Figure 2.- The semispan 47.5° sweptback wing mounted on the reflection plane.

[redacted]

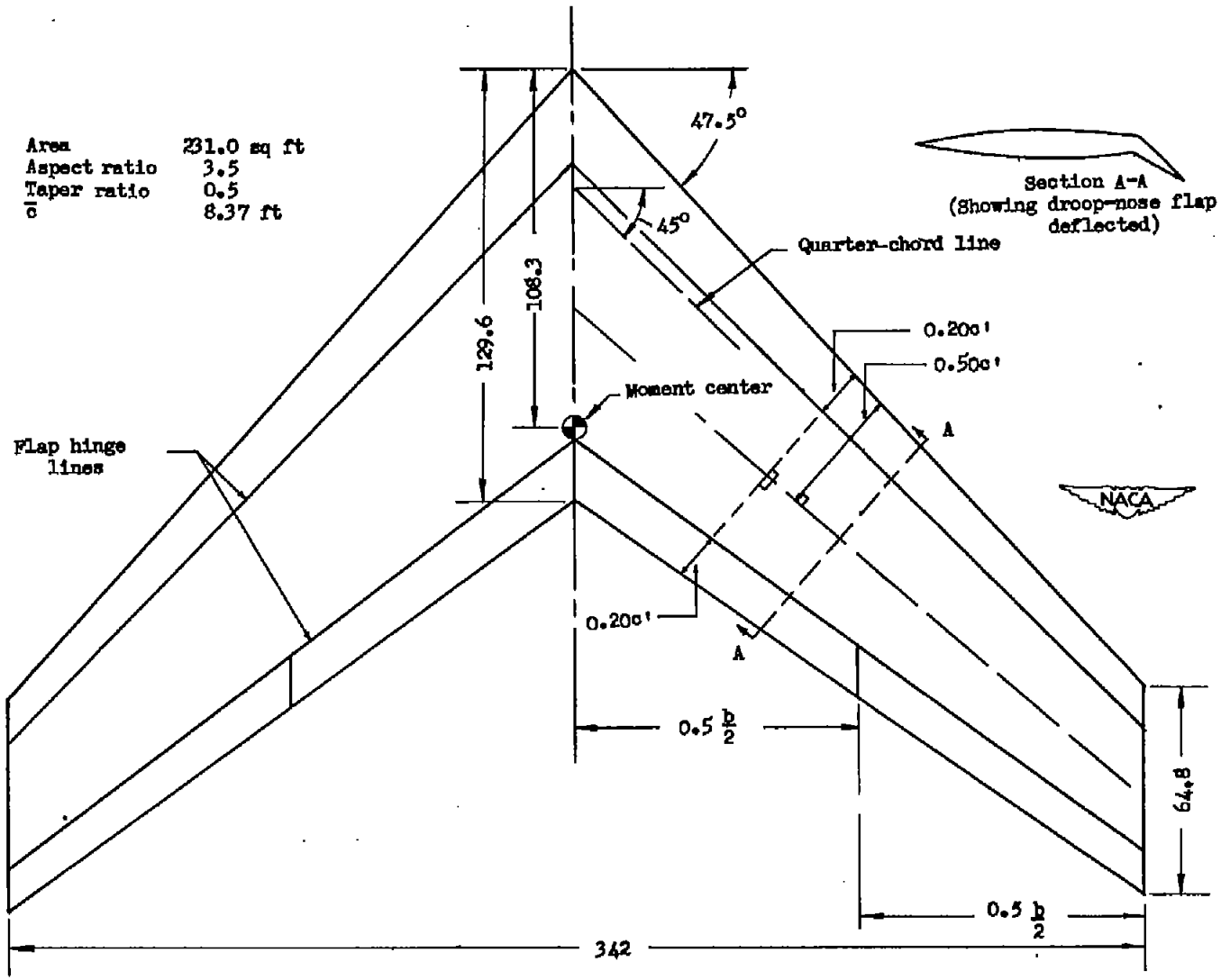

Figure 3.- Plan form of 47.5° sweptback wing. All dimensions are given in inches.

Pressure orifice locations, percent chord	
Upper surface	Lower surface
2.5	5.0
7.5	15.0
15.0	30.0
18.5	42.5
22.5	52.5
32.5	75.0
42.5	85.0
52.5	95.0
62.5	
75.0	
85.0	
92.5	
97.5	

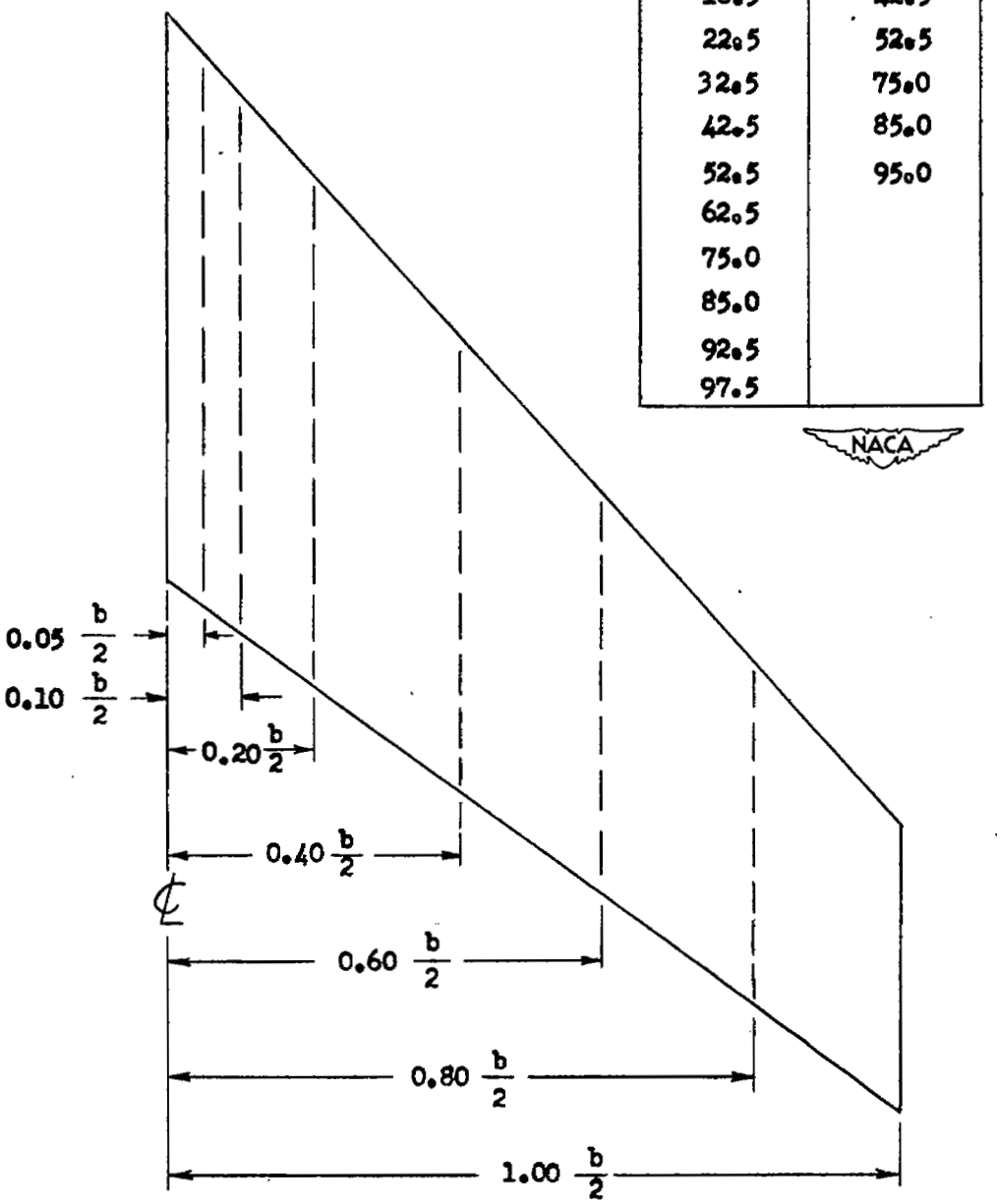

Figure 4.- Spanwise and chordwise locations of the pressure orifices.

[redacted]

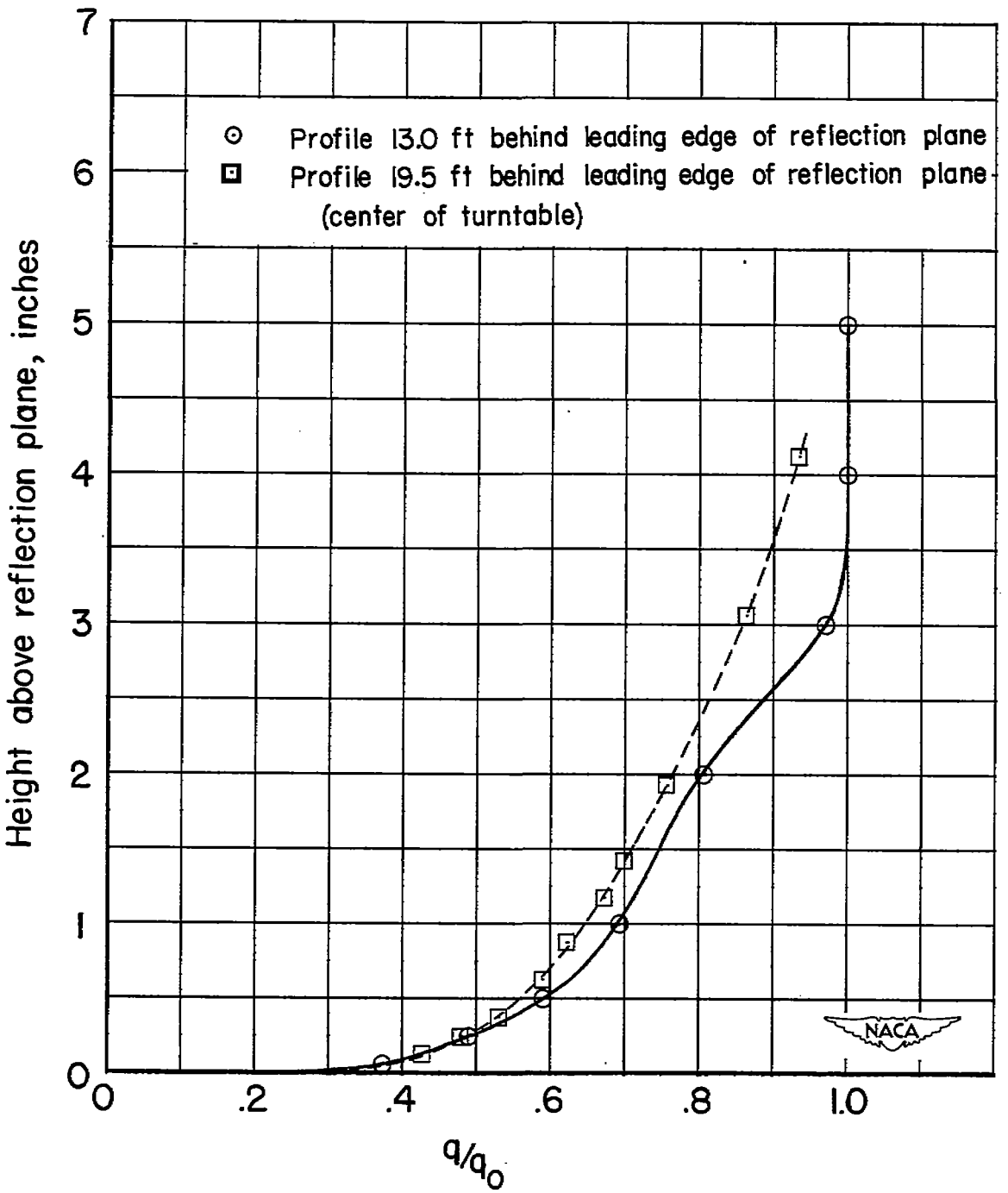

Figure 5.- Boundary-layer profiles on reflection plane at two stations; wing at $\alpha = -0.3^{\circ}$.

[redacted]

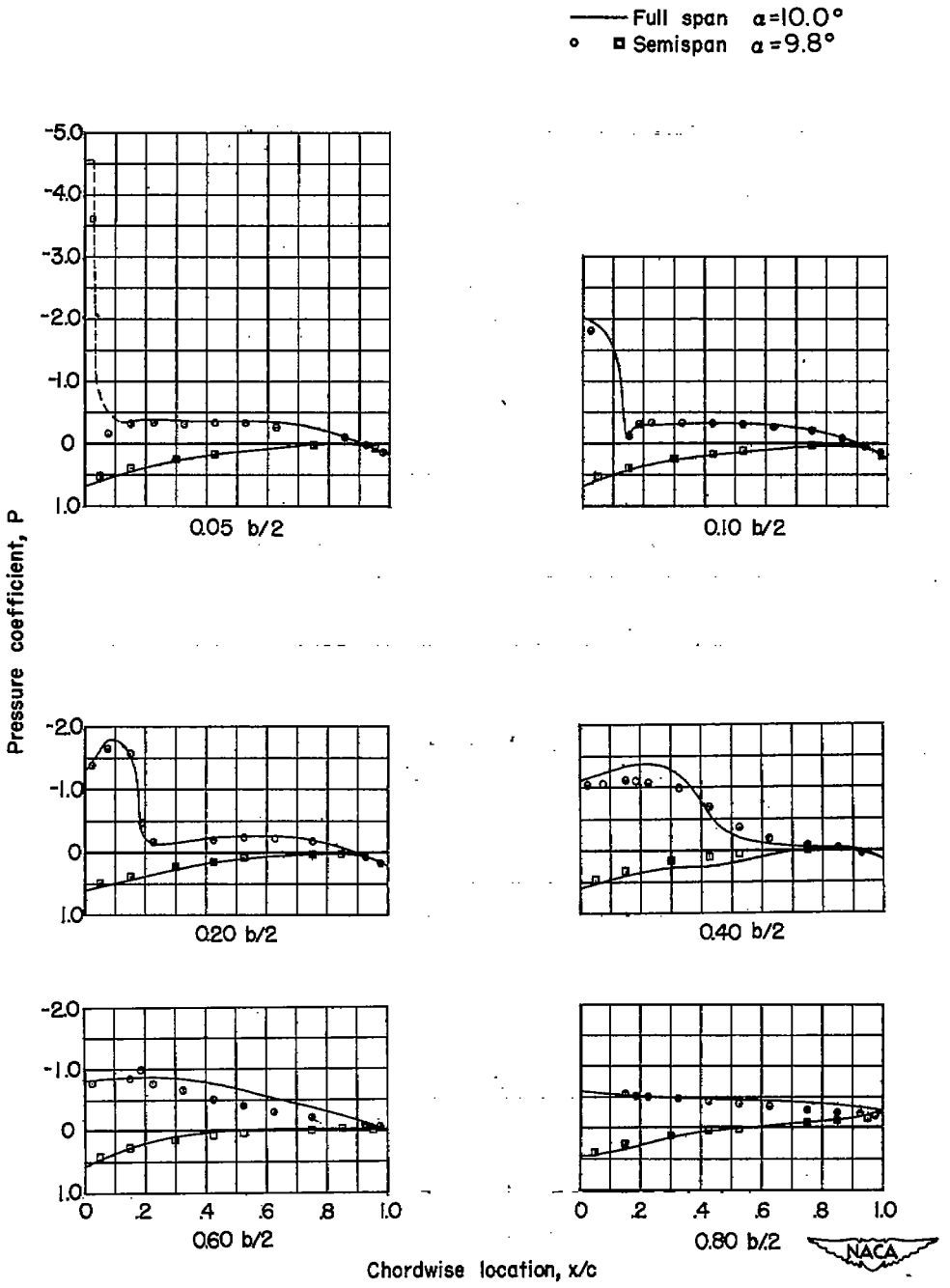

Figure 6.- Chordwise pressure distribution at six spanwise stations. Basic wing.

[redacted]

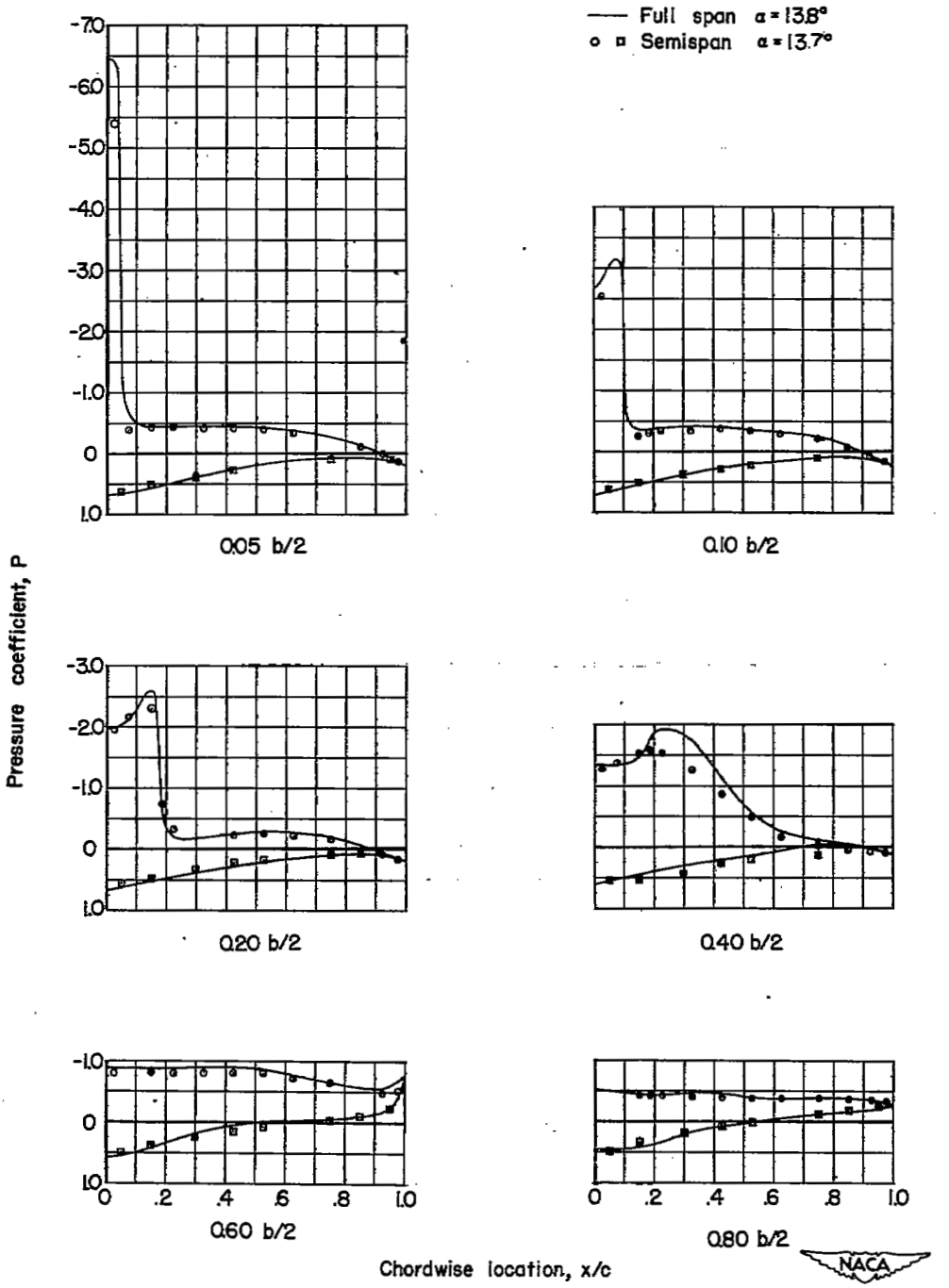

Figure 6.- Continued.

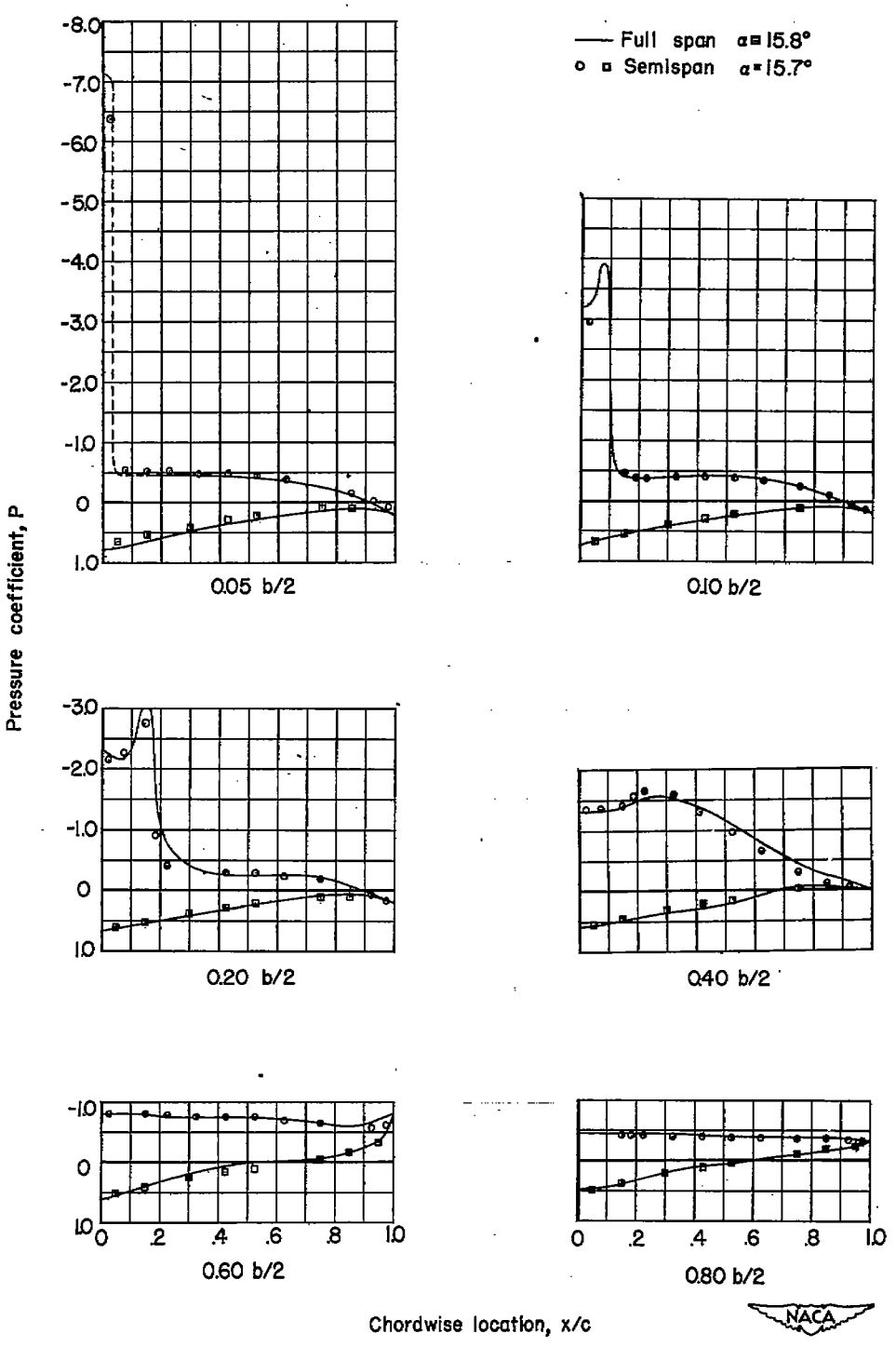

Figure 6.- Continued.

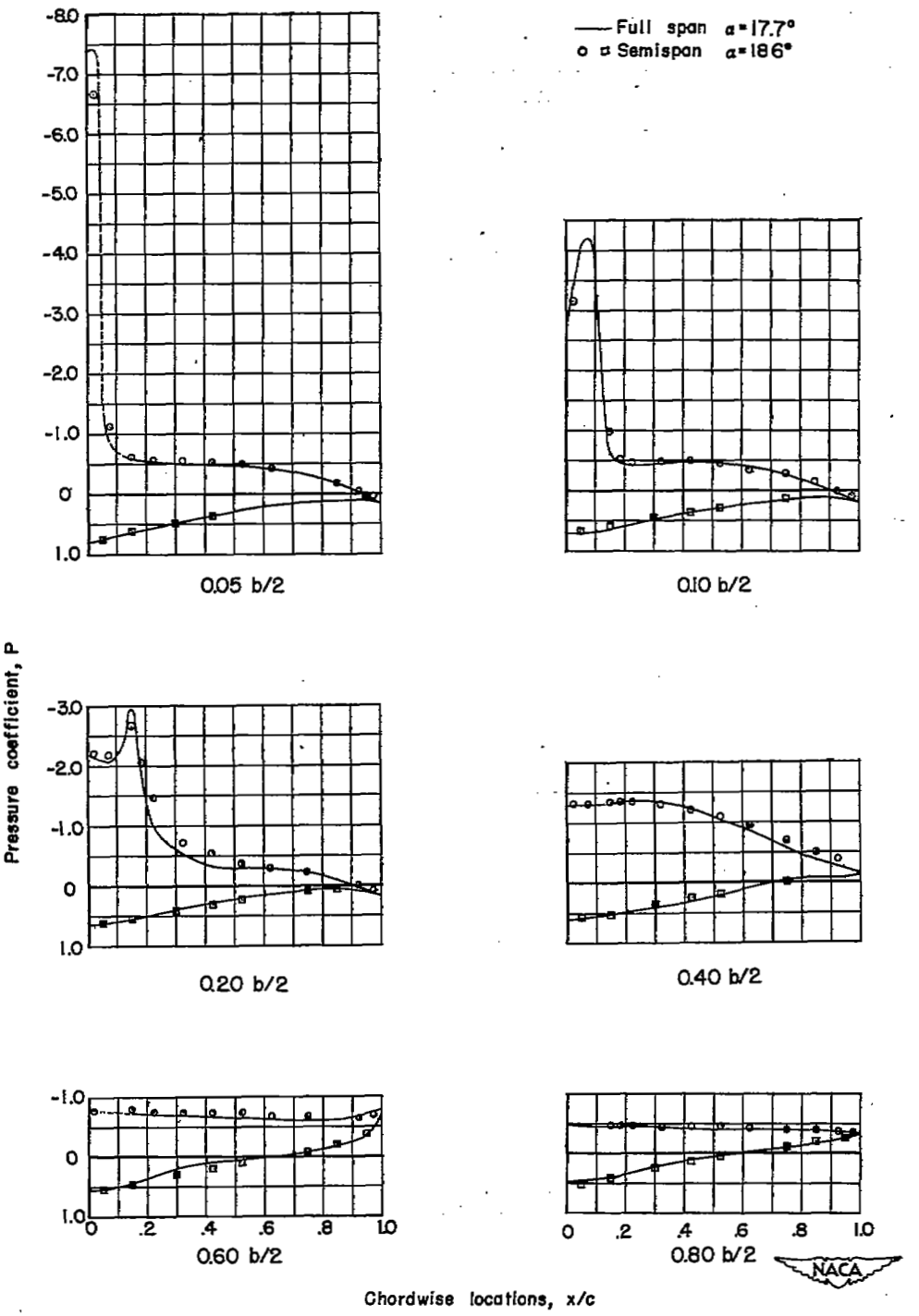

Figure 6.- Concluded.

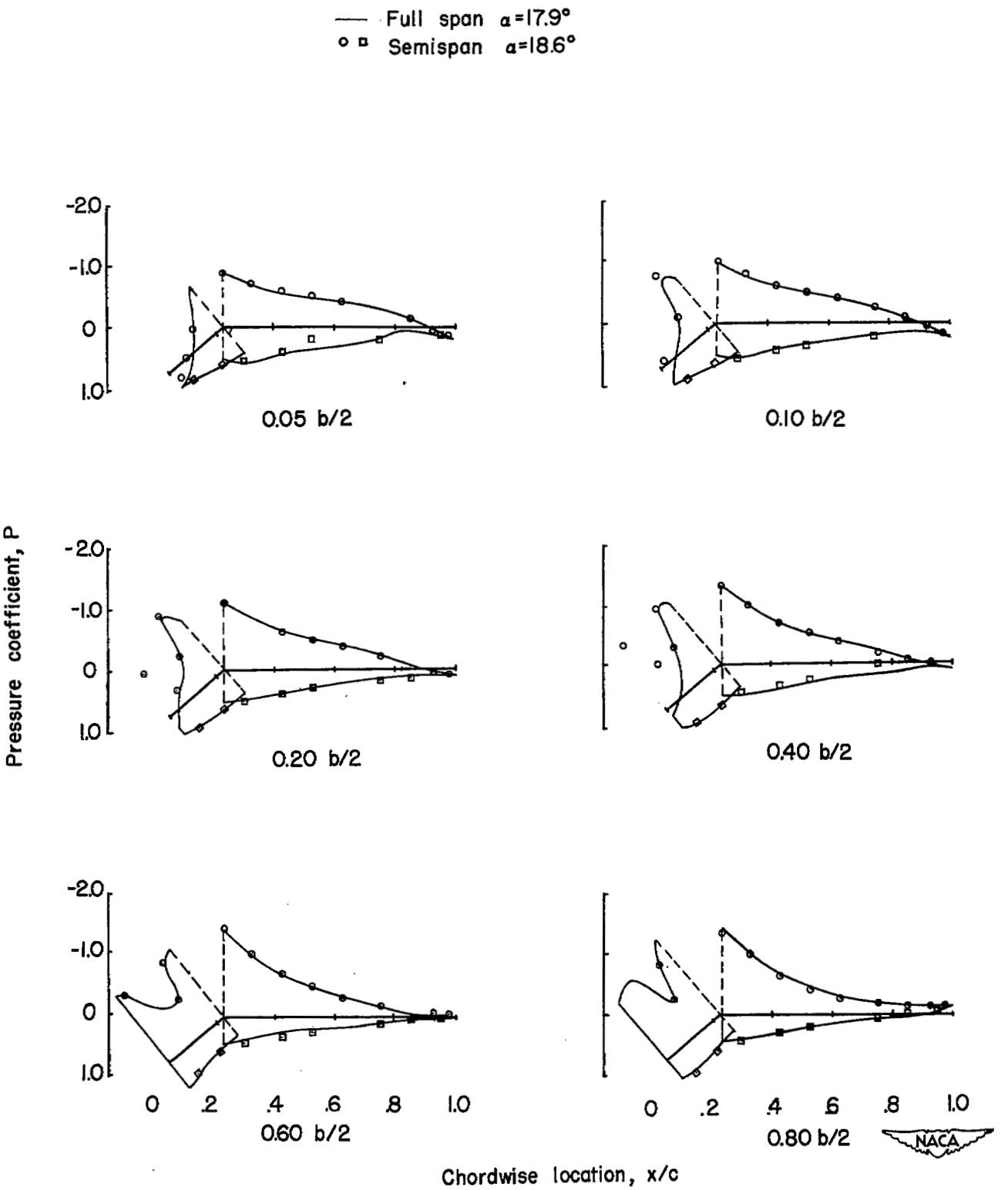

Figure 7.- Chordwise pressure distribution at six spanwise stations. Wing with 1.00b/2 drooped-nose flap deflected 40°.

[redacted]

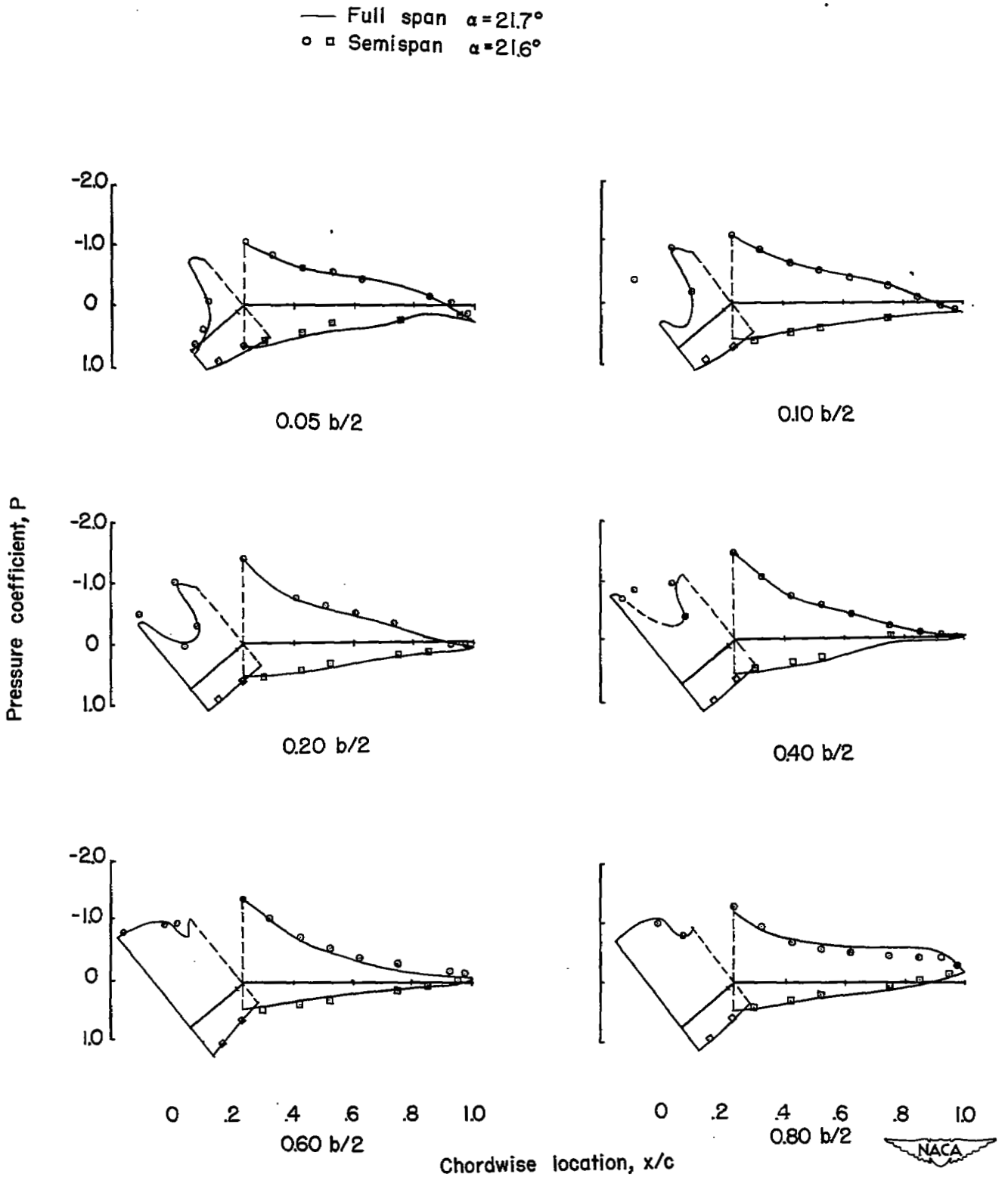

Figure 7.- Concluded.

[redacted]

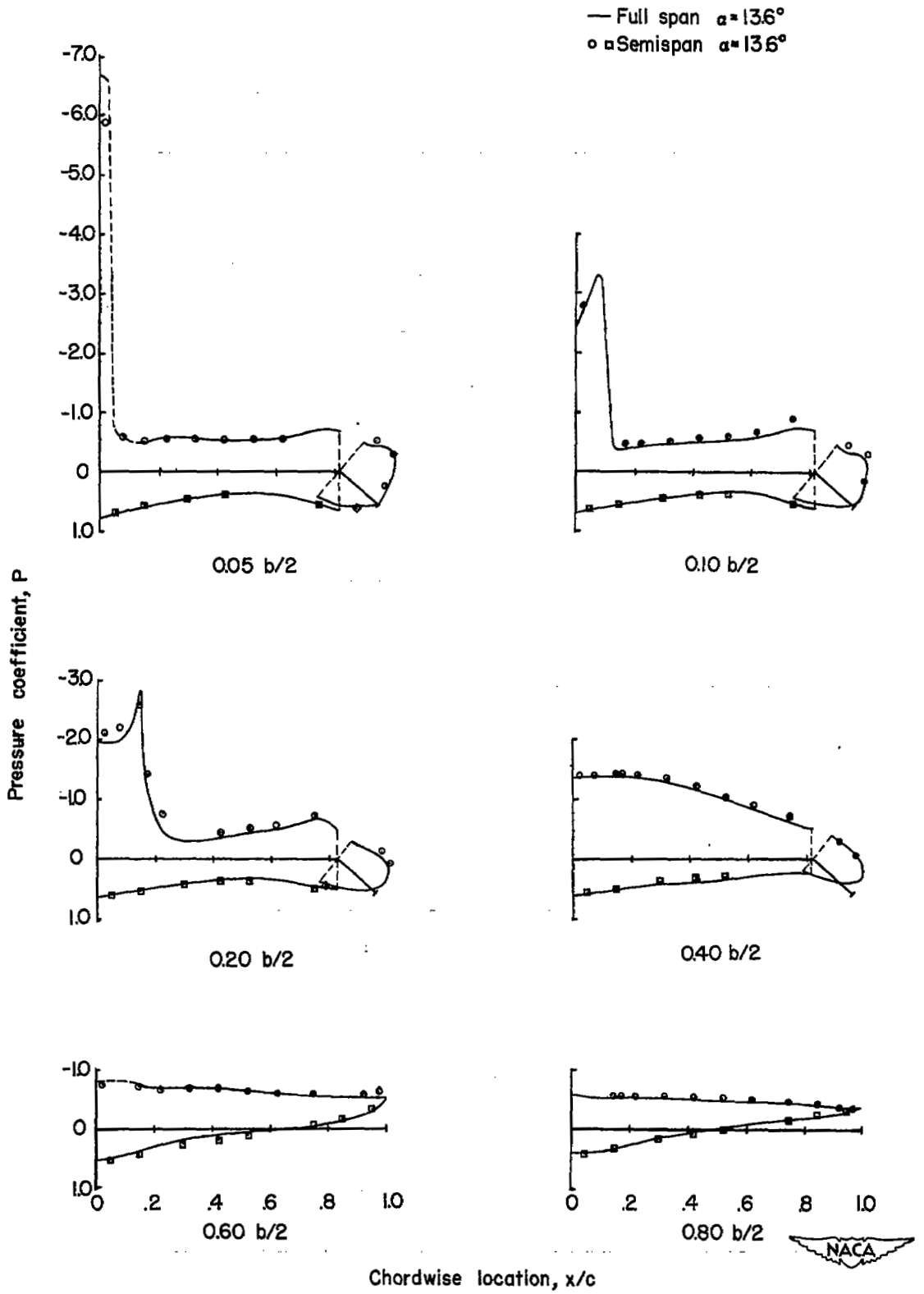

Figure 8.- Chordwise pressure distribution at six spanwise stations. Wing with 0.50b/2 trailing-edge flap deflected 40°.

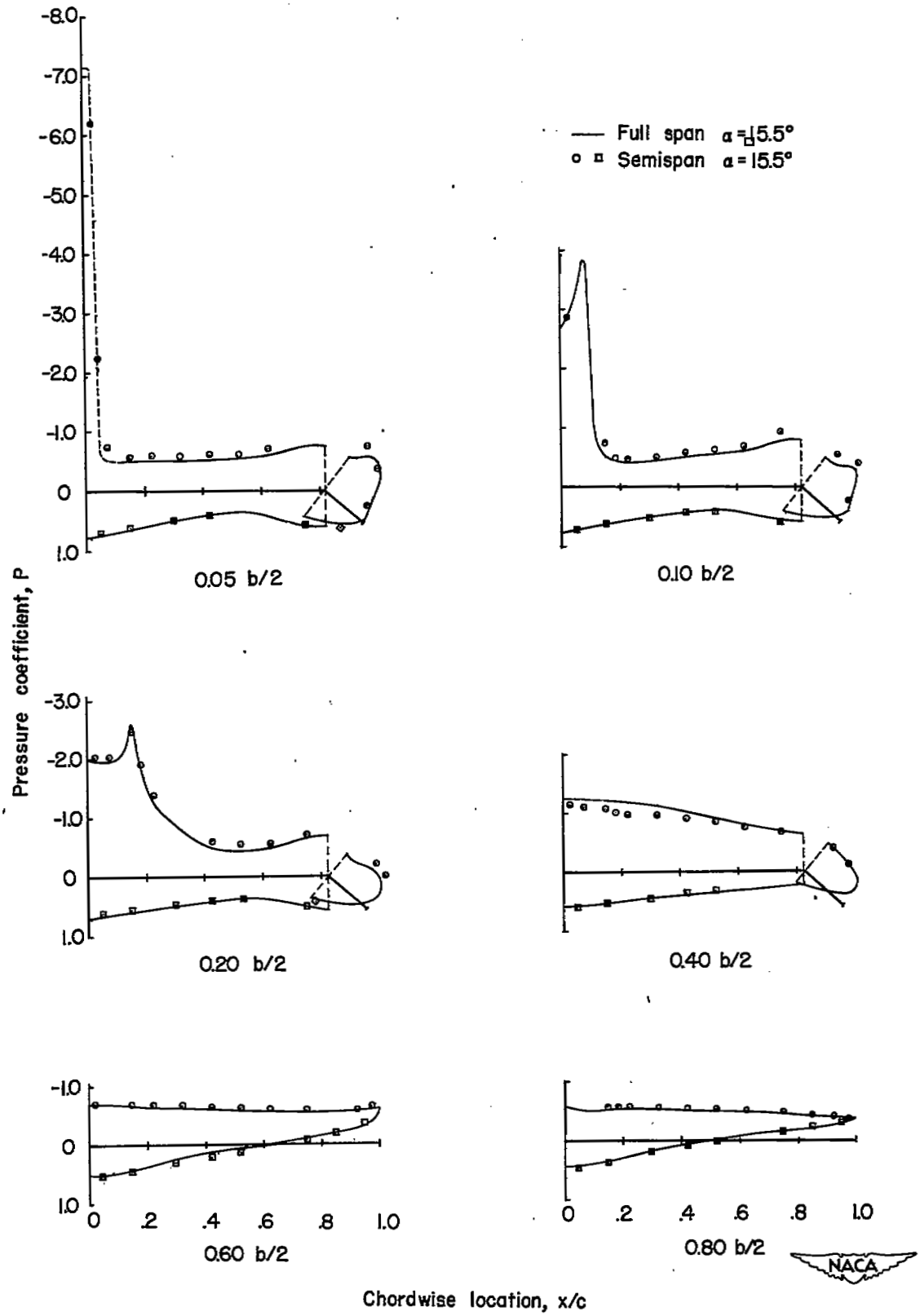

Figure 8.- Concluded.

[redacted]

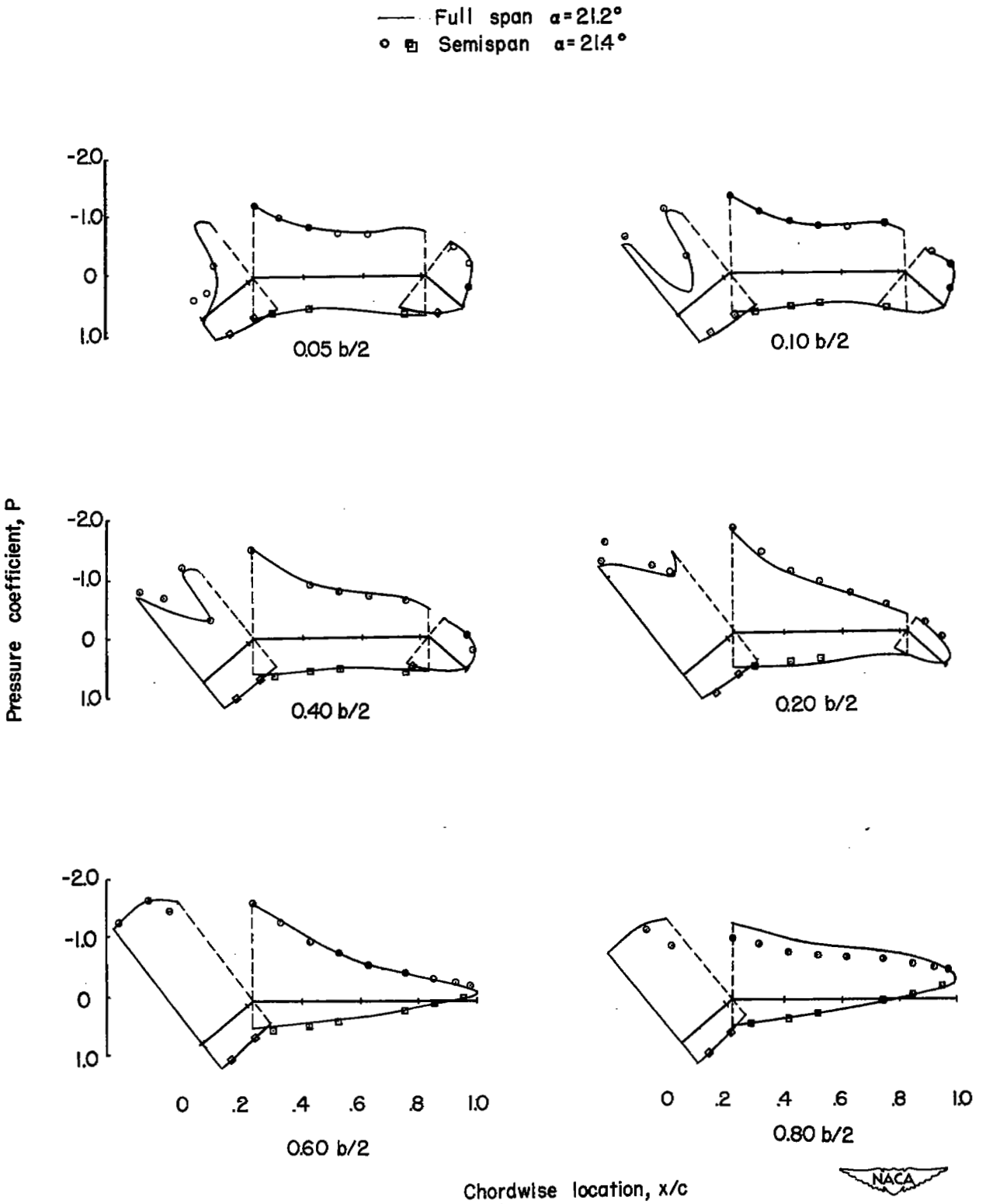

Figure 9.- Chordwise pressure distribution at six spanwise stations. Wing with 0.50b/2 trailing-edge flap and 1.00b/2 drooped-nose flap deflected 40°.

[redacted]

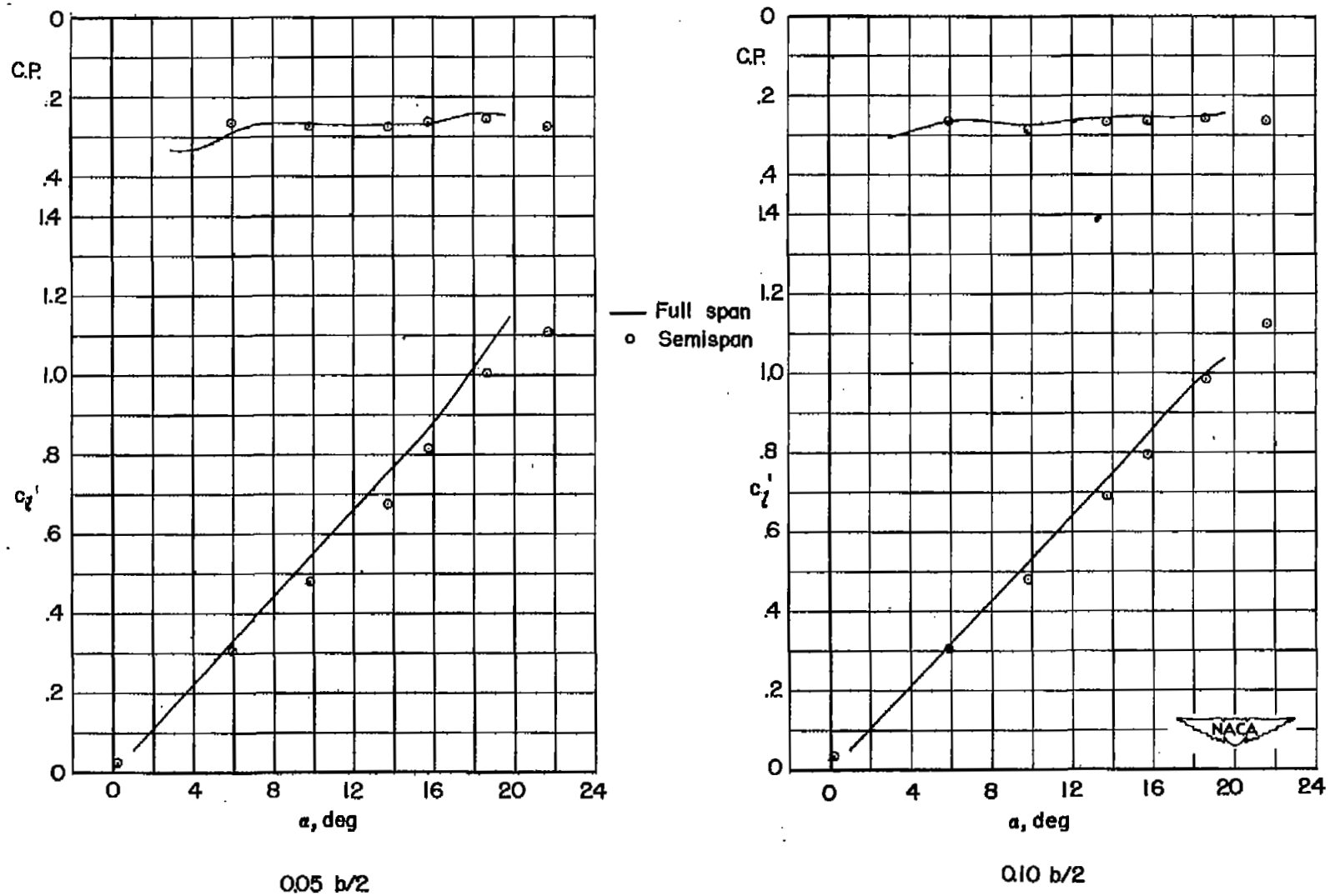

Figure 10.- Variation of section lift coefficient and center-of-pressure location with angle of attack for six spanwise stations. Basic wing.

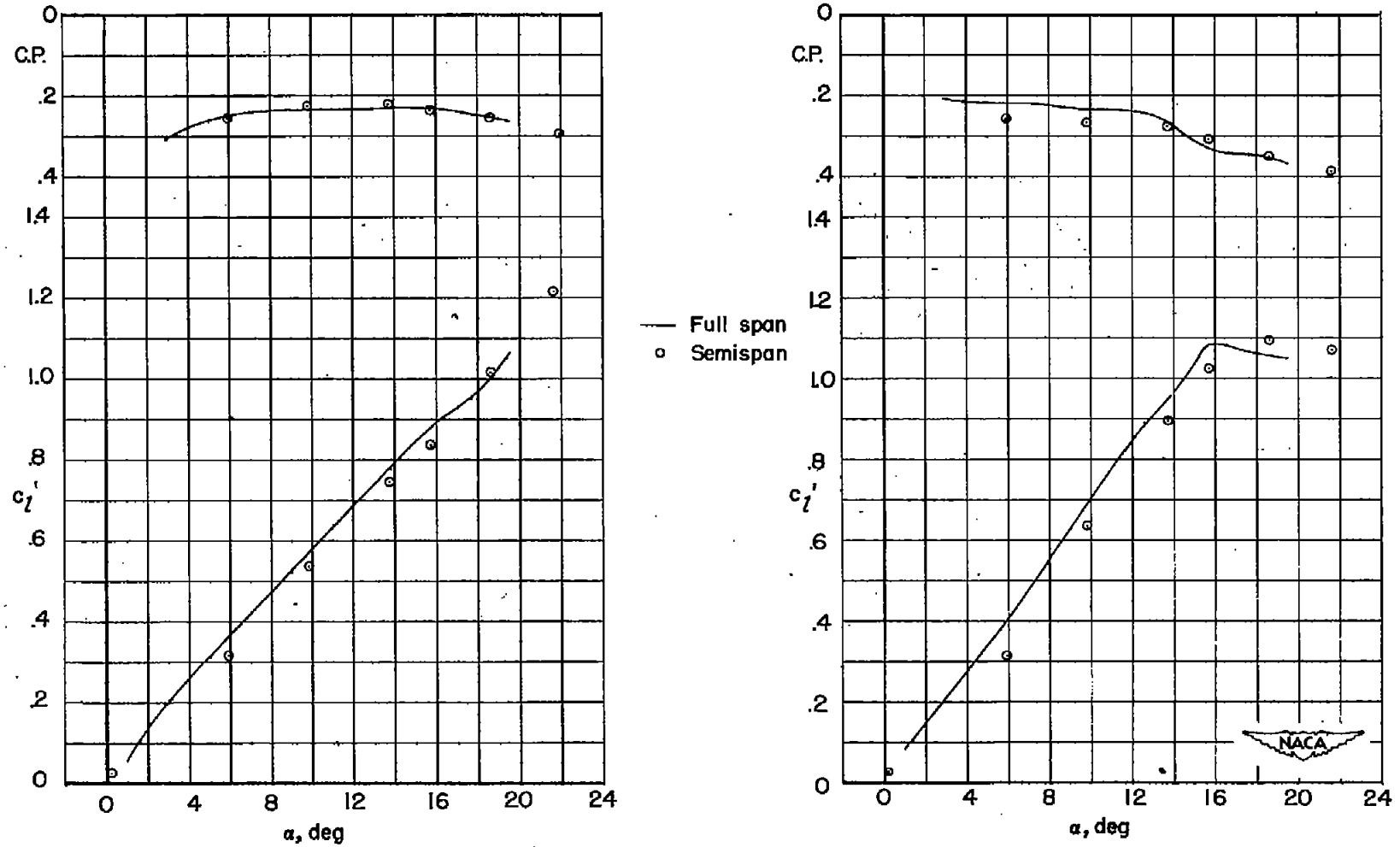

Figure 10.- Continued.

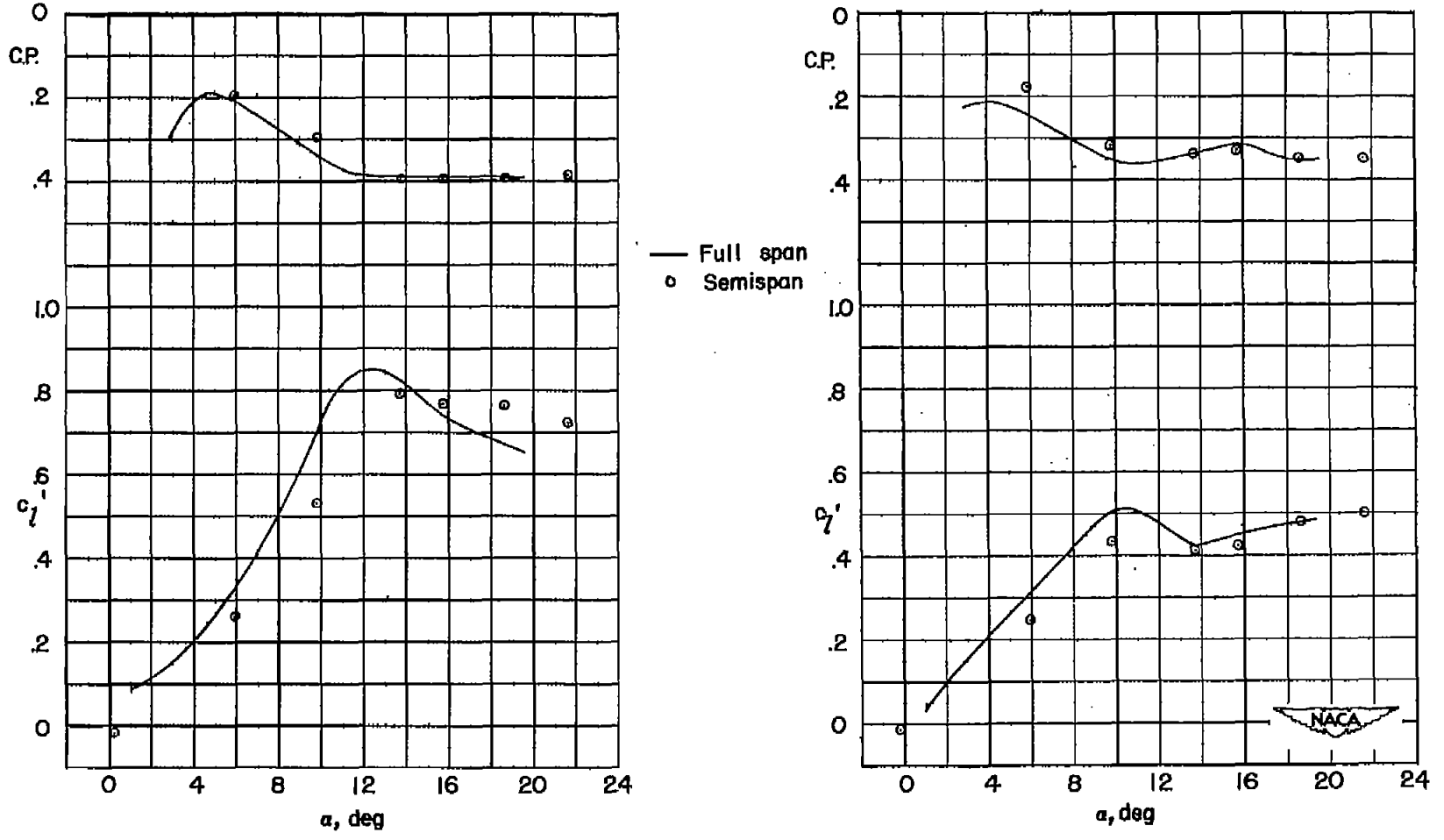

Figure 10.- Concluded.

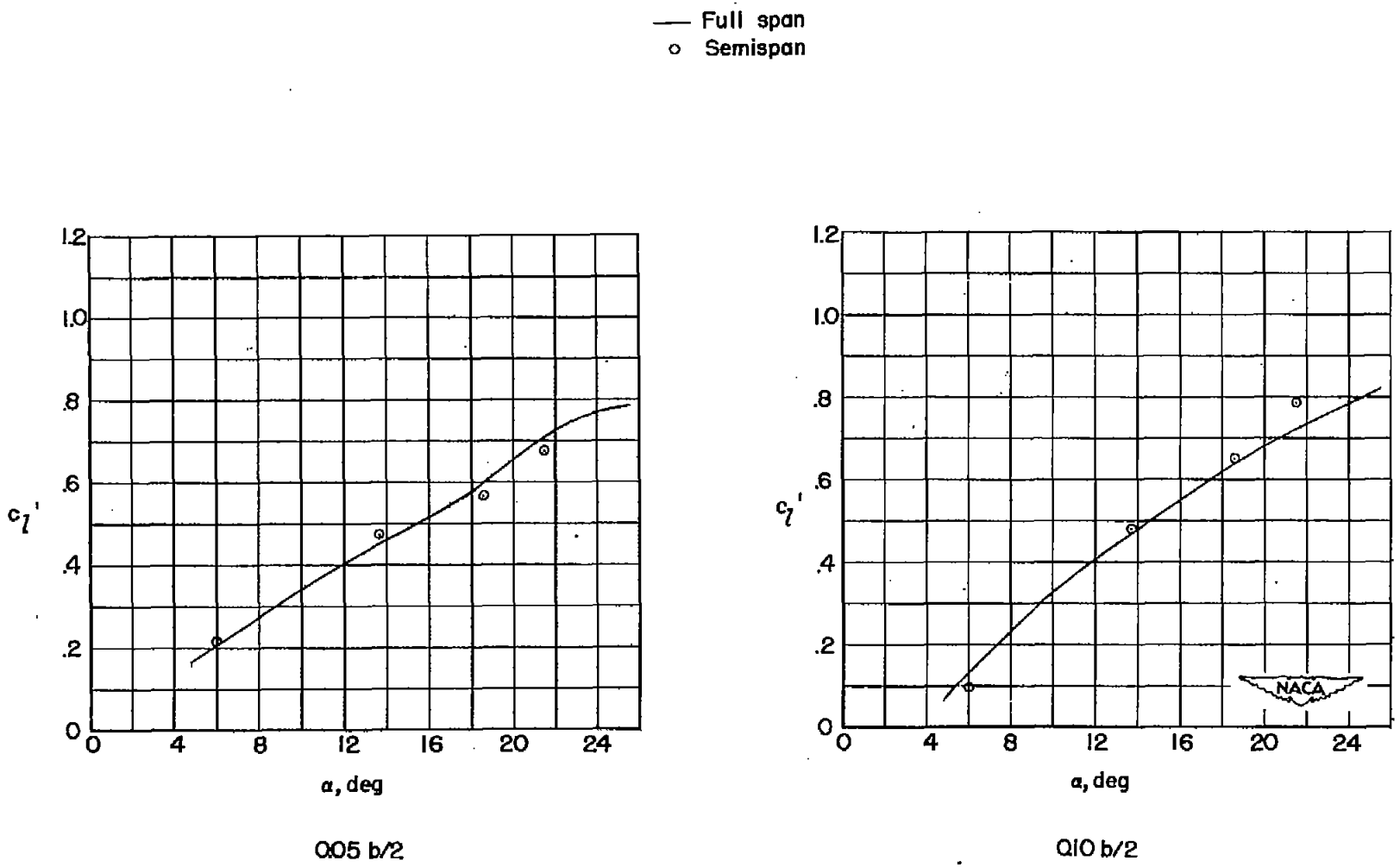

Figure 11.- Variation of section lift coefficient with angle of attack for six spanwise stations. Wing with 1.00b/2 drooped-nose flap deflected 40°.

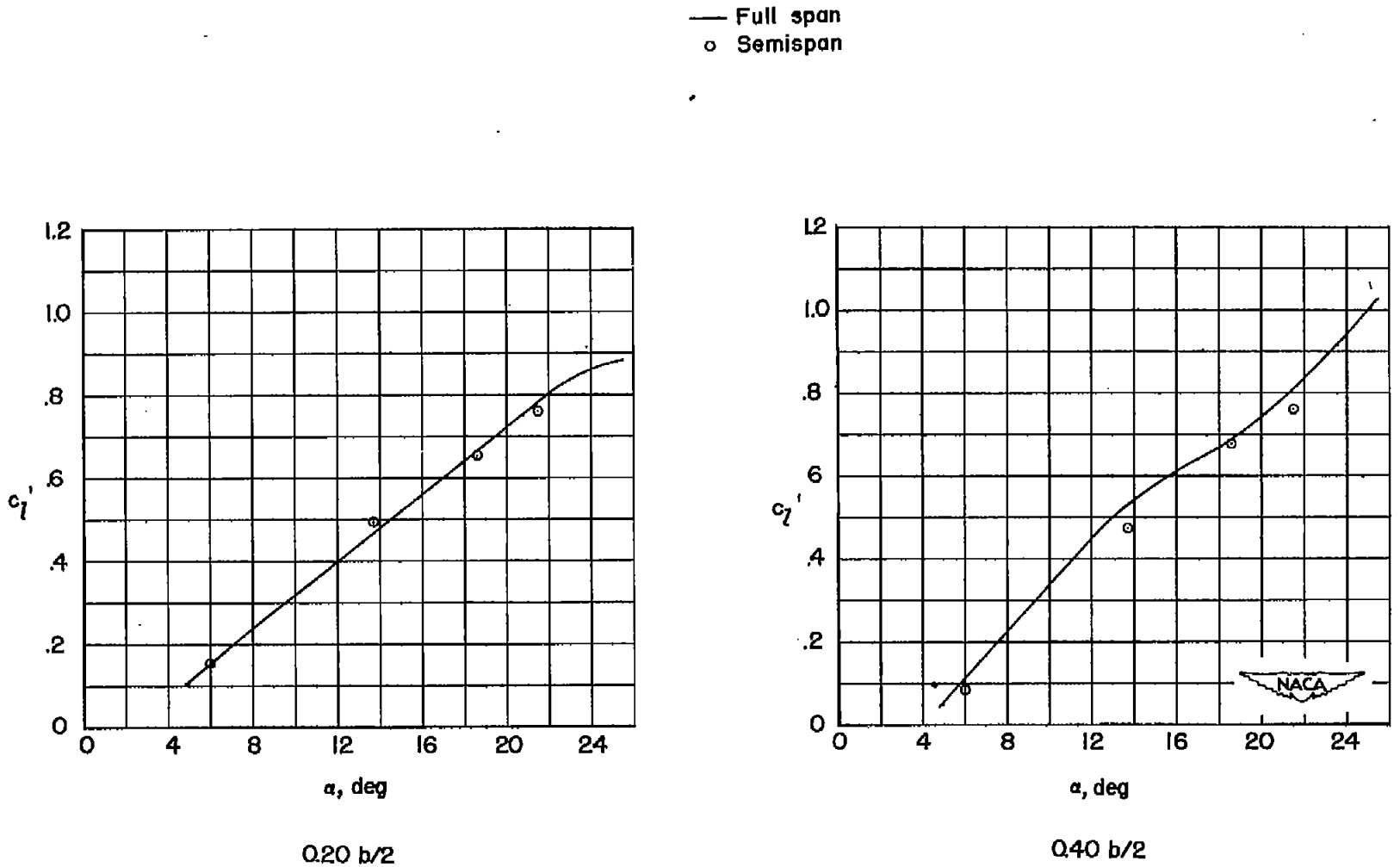

Figure 11.- Continued.

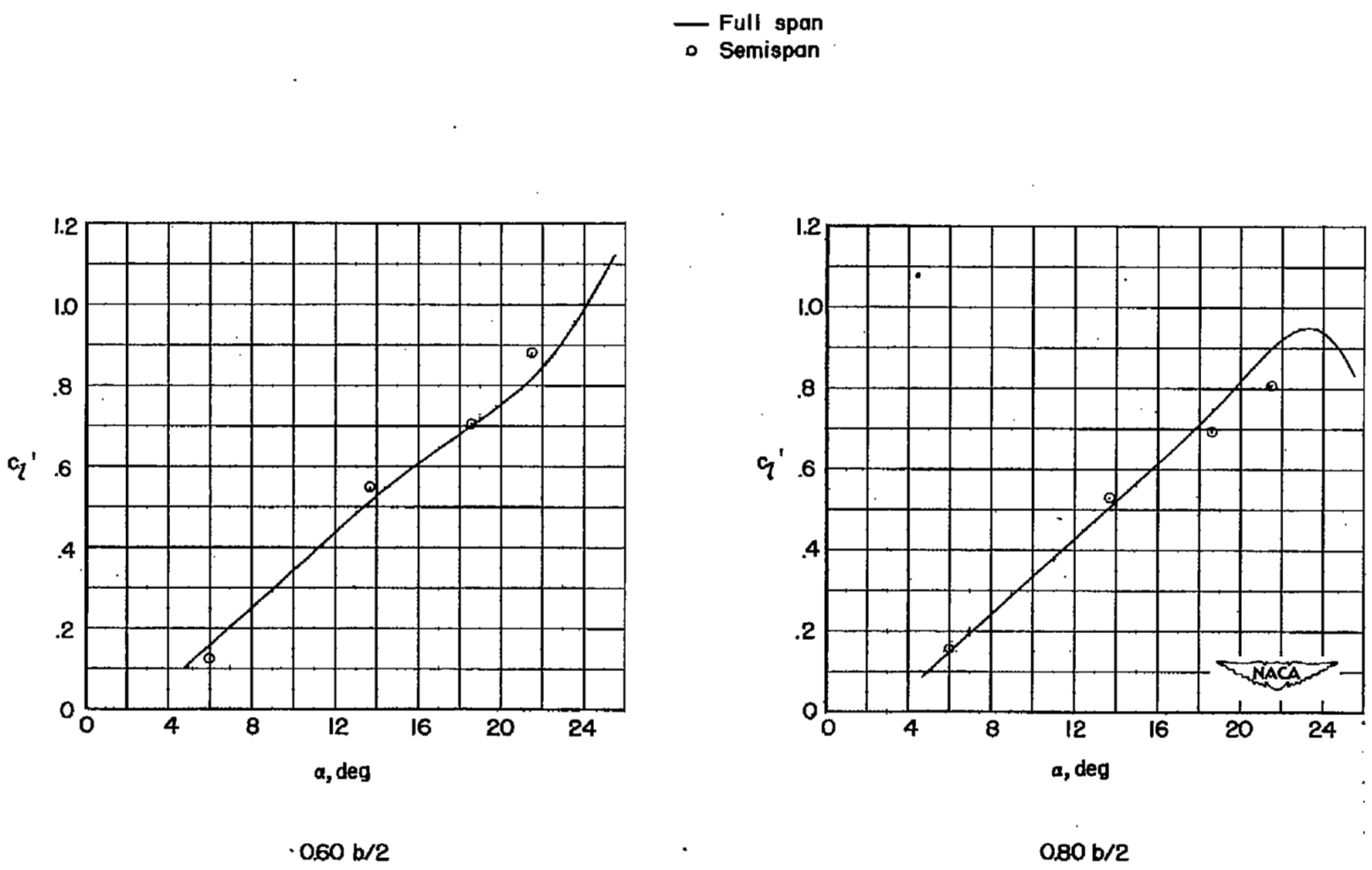

Figure 11.- Concluded.

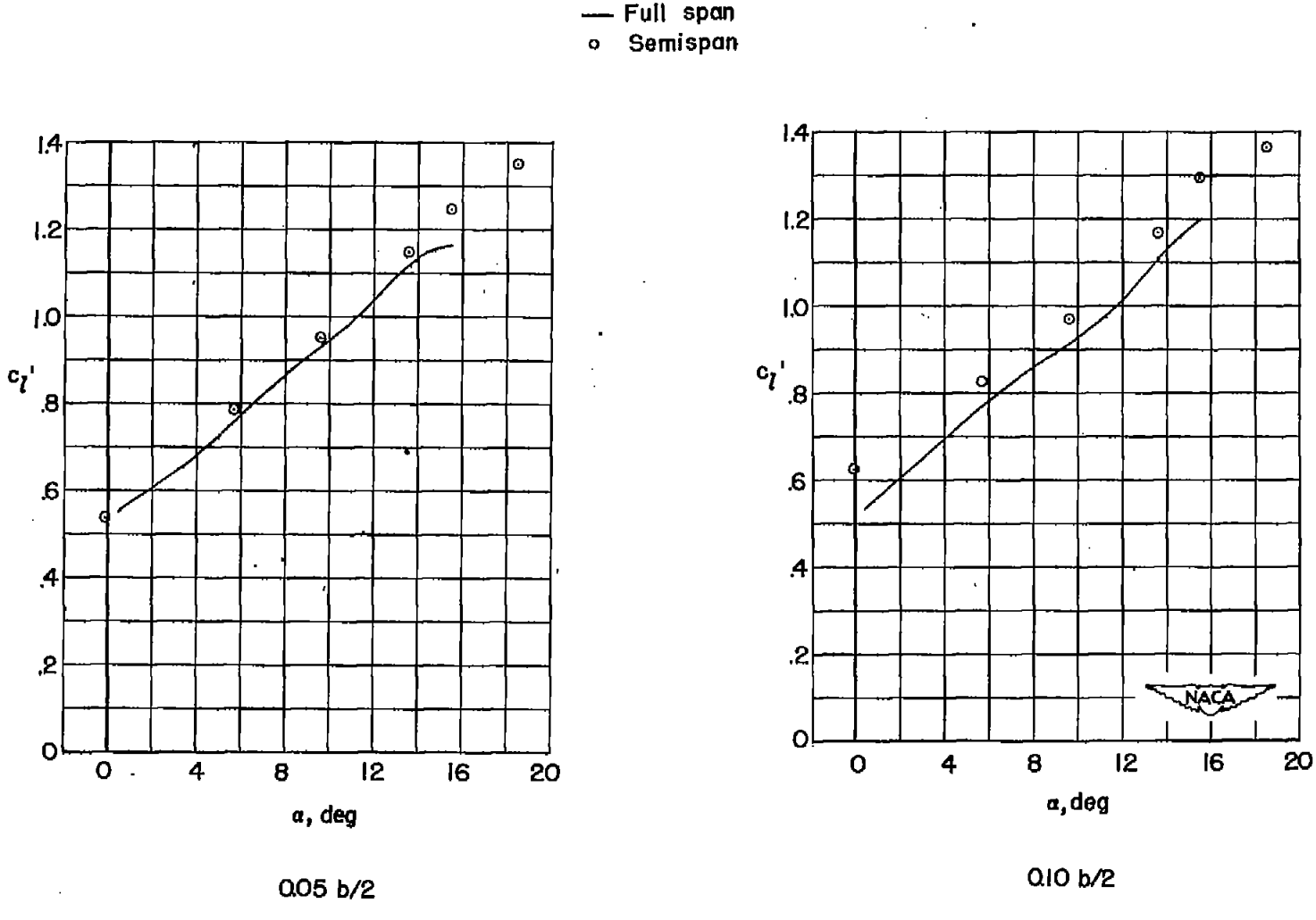

Figure 12.- Variation of section lift coefficient with angle of attack for six spanwise stations. Wing with 0.50b/2 trailing-edge flap deflected 40°.

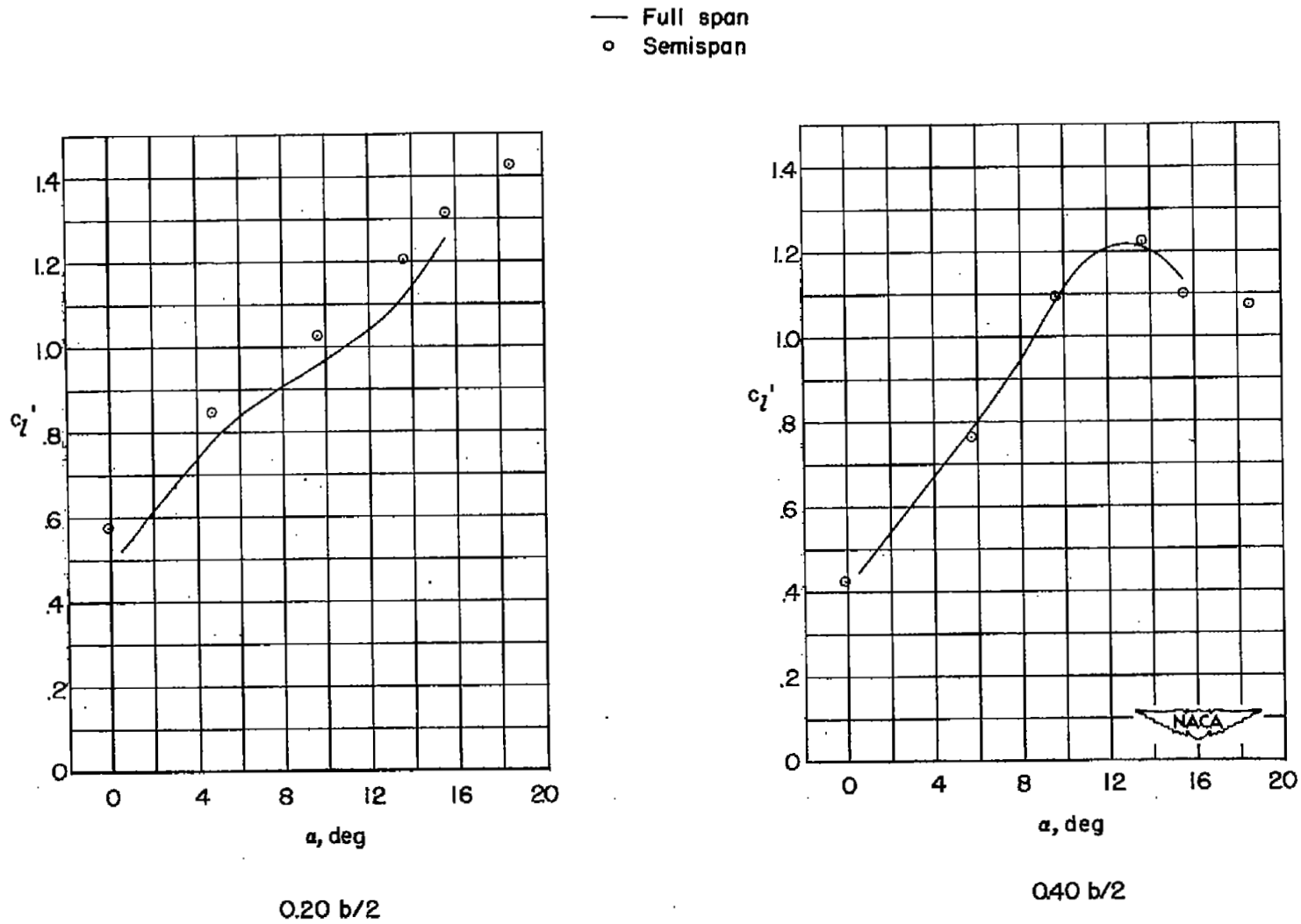

Figure 12.- Continued.

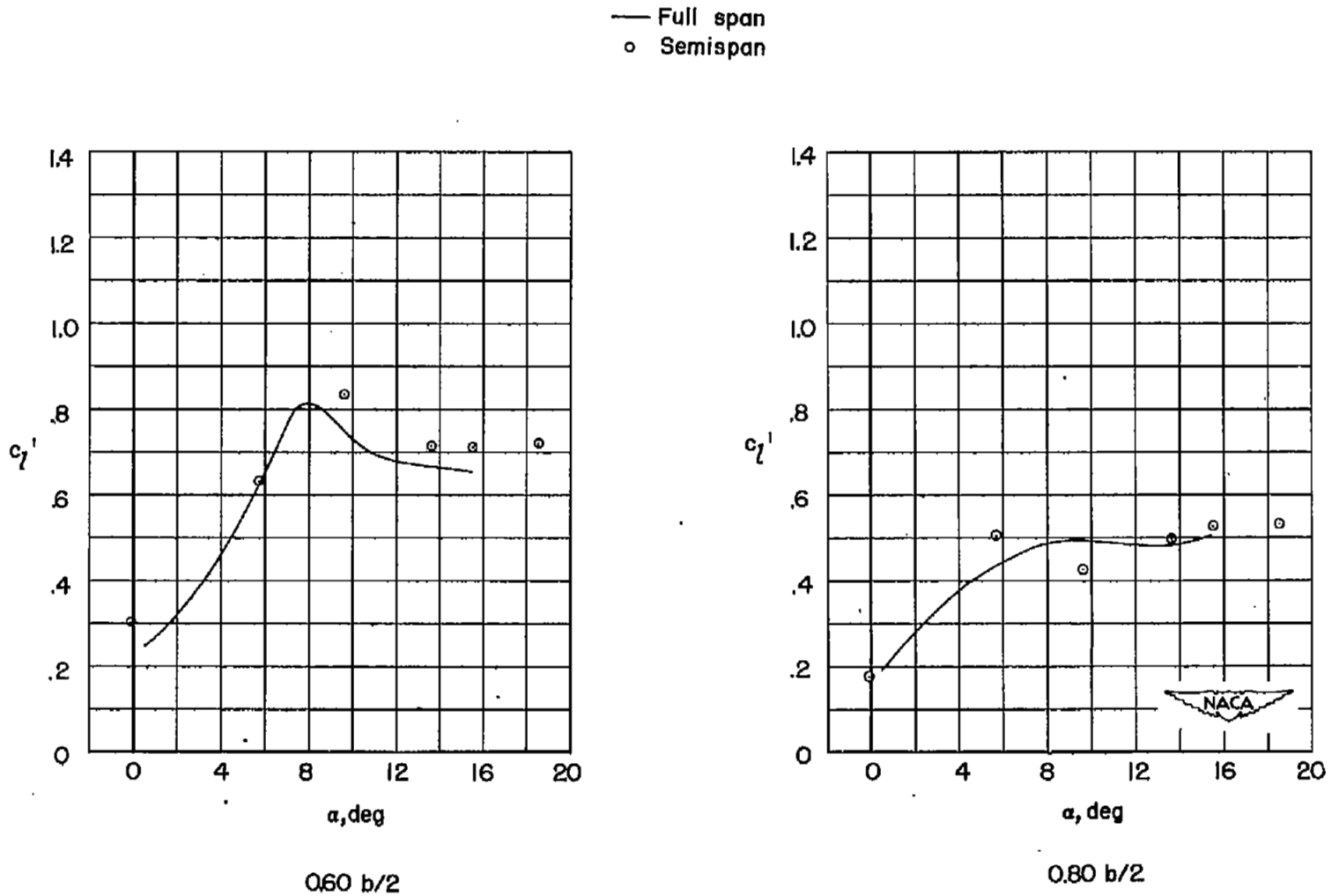

Figure 12.- Concluded.

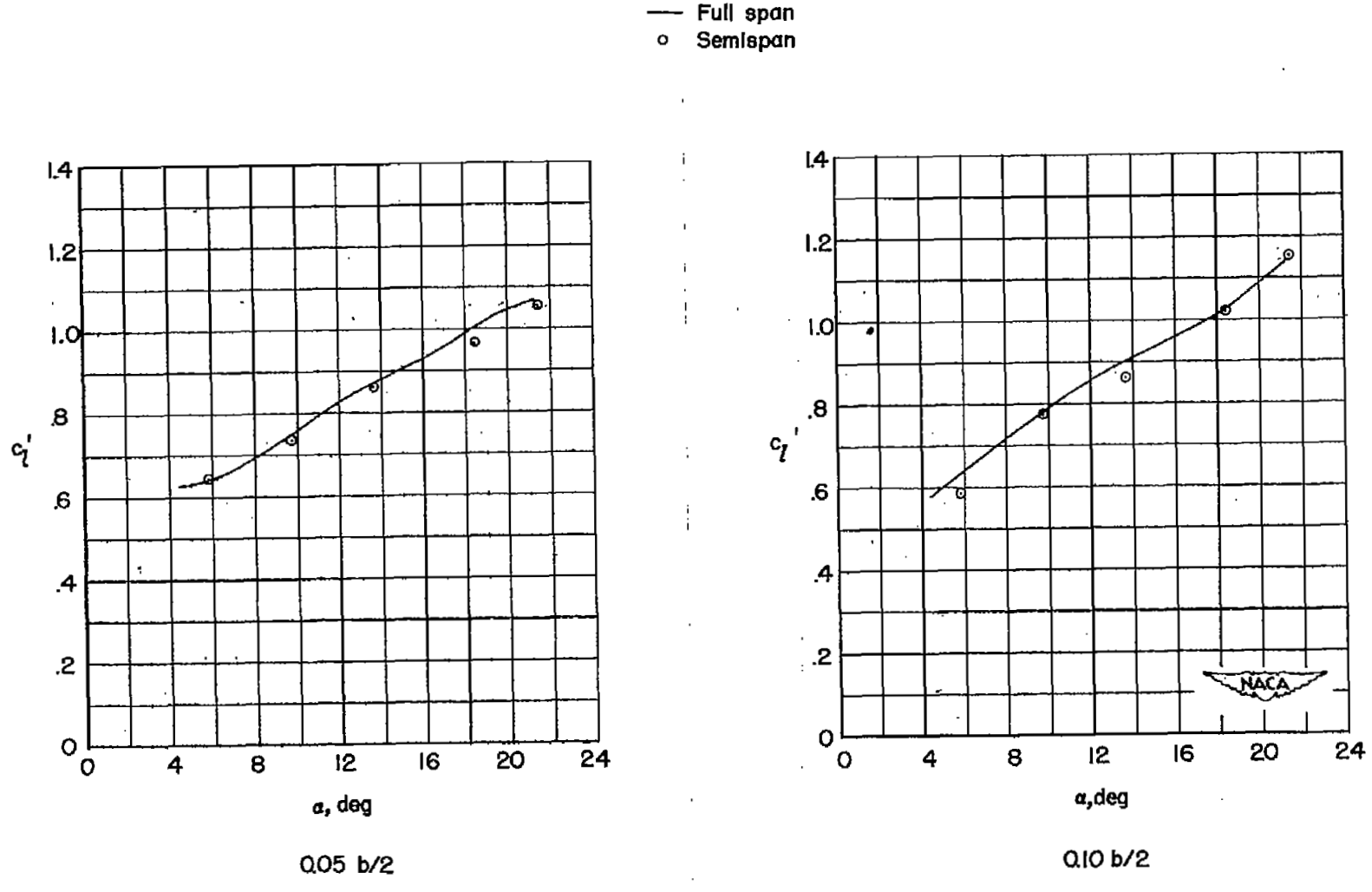

Figure 13.- Variation of section lift coefficient with angle of attack for six spanwise stations. Wing with 0.50b/2 trailing-edge flap and 1.00b/2 drooped-nose flap deflected 40°.

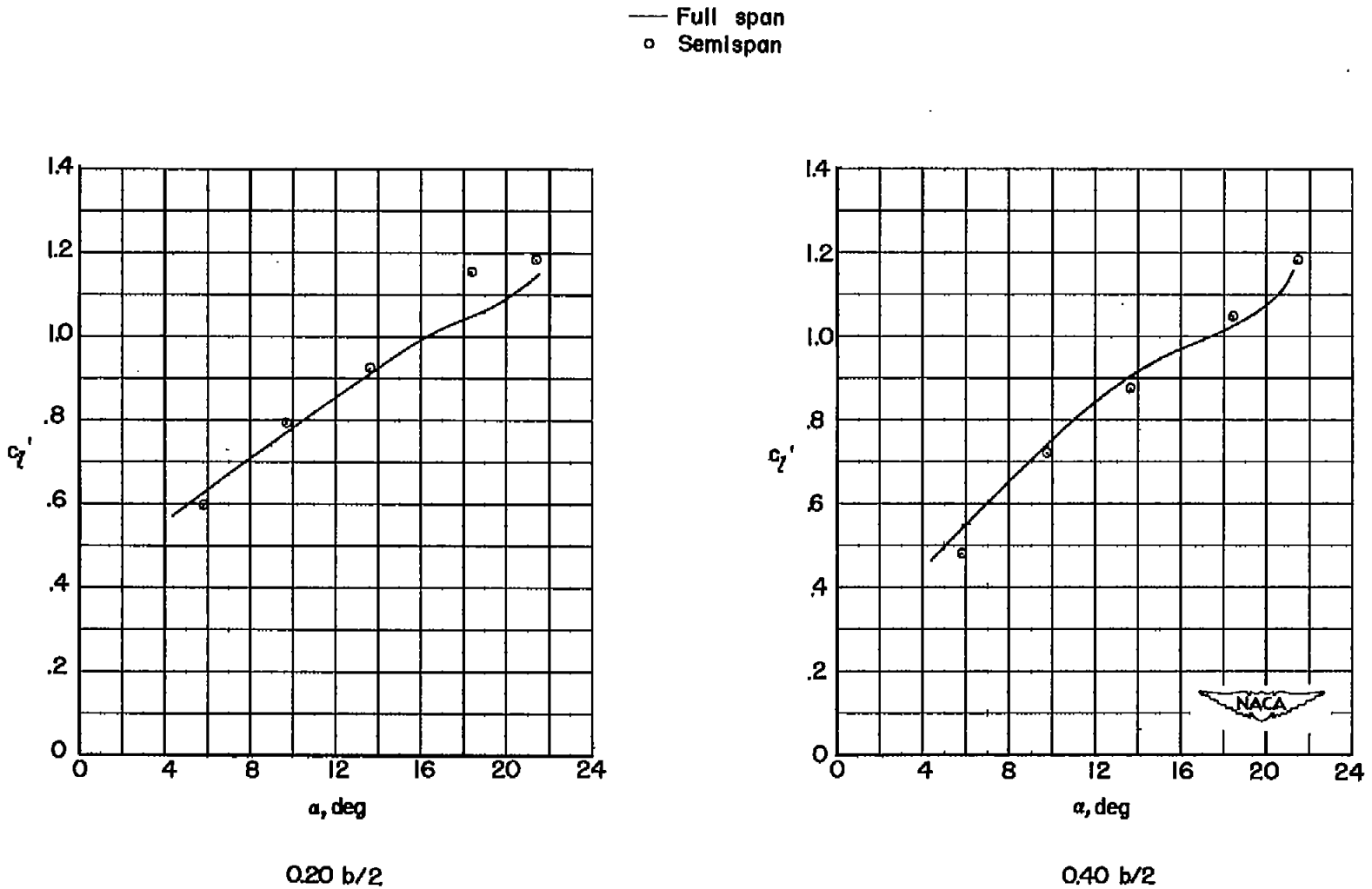

Figure 13.- Continued.

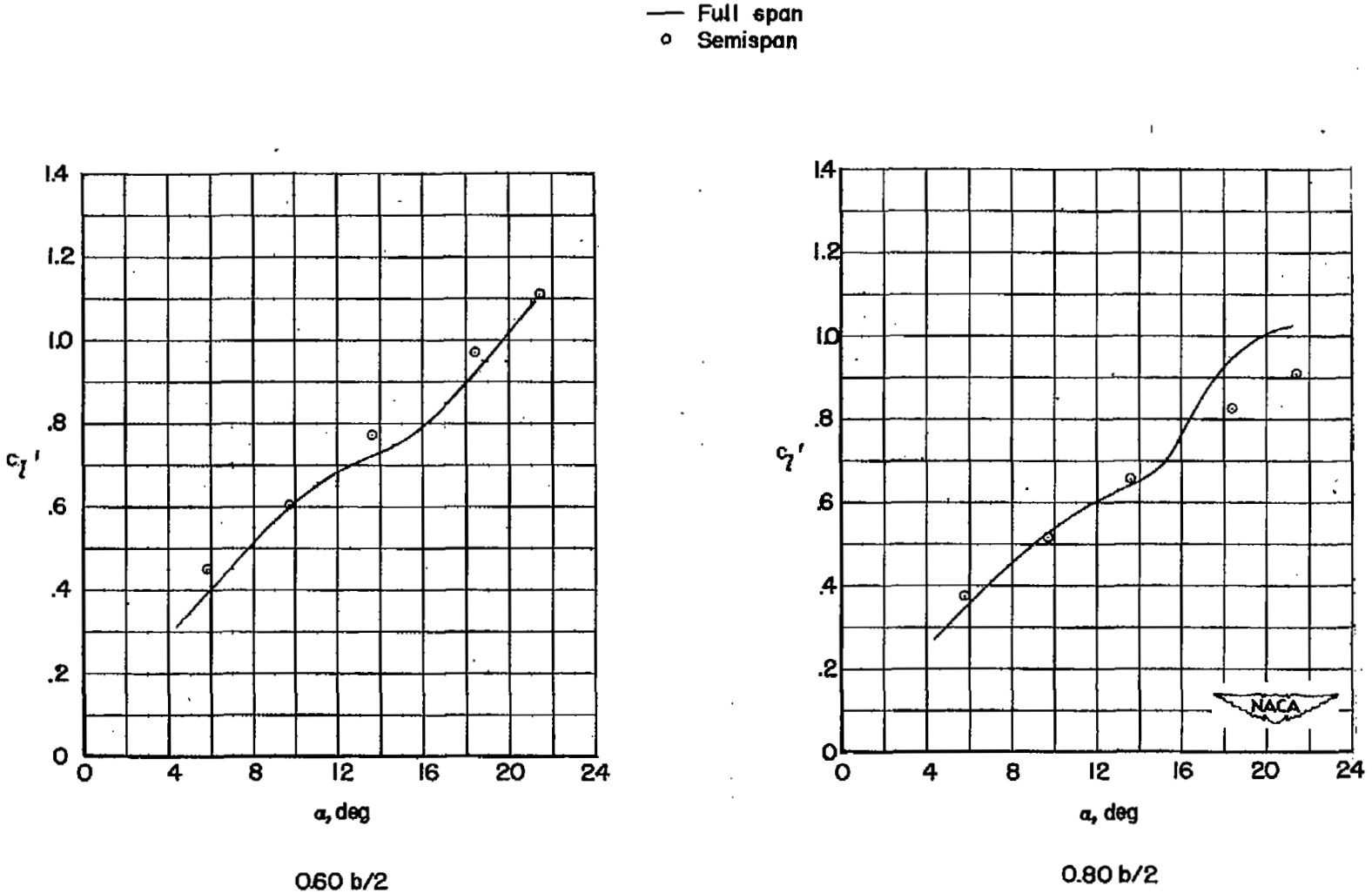

Figure 13.- Concluded.

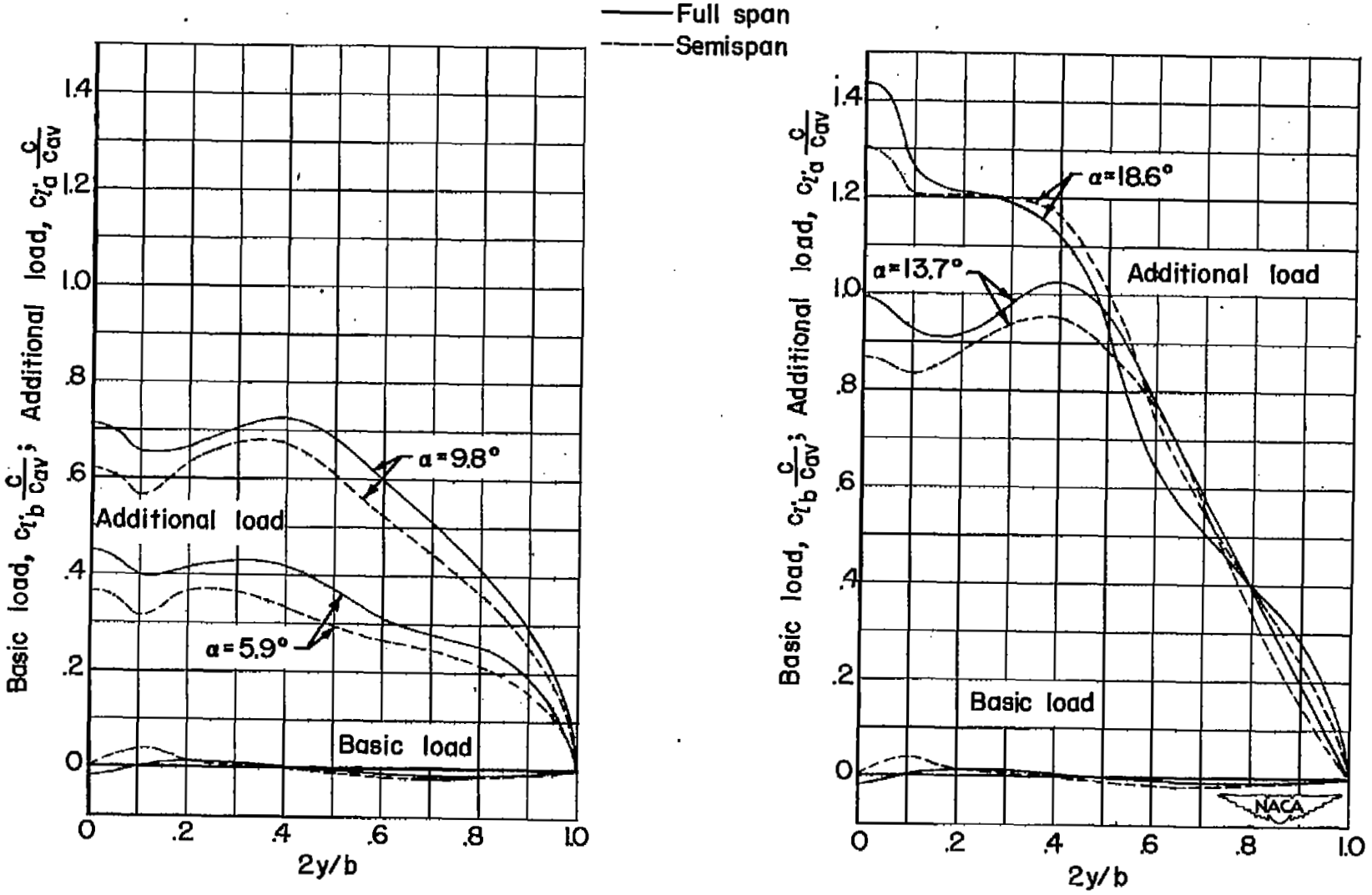

Figure 14.- Additional and basic load at several angles of attack. Basic wing.

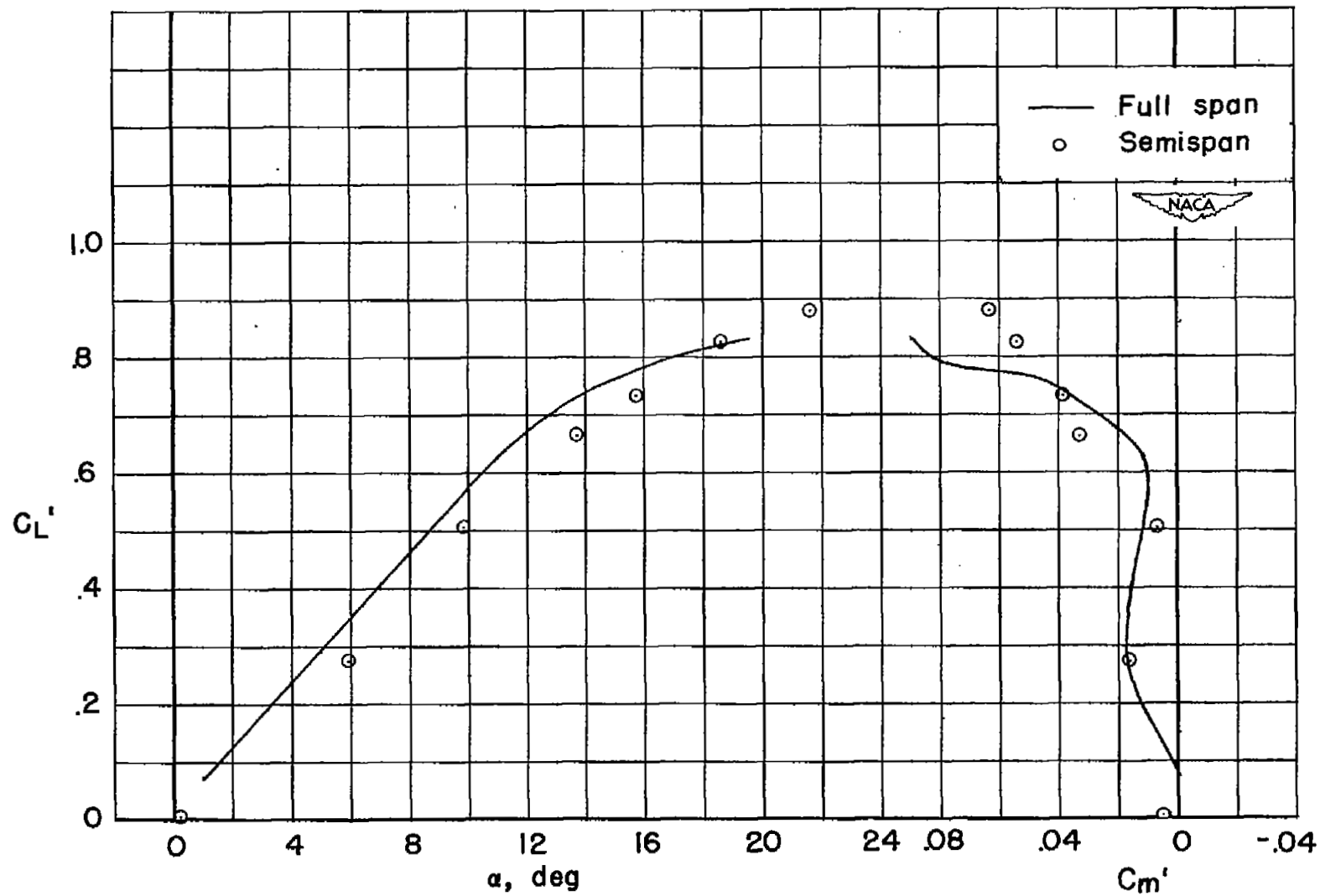

Figure 15.- Variation of wing lift coefficient with angle of attack and pitching-moment coefficient. Basic wing.

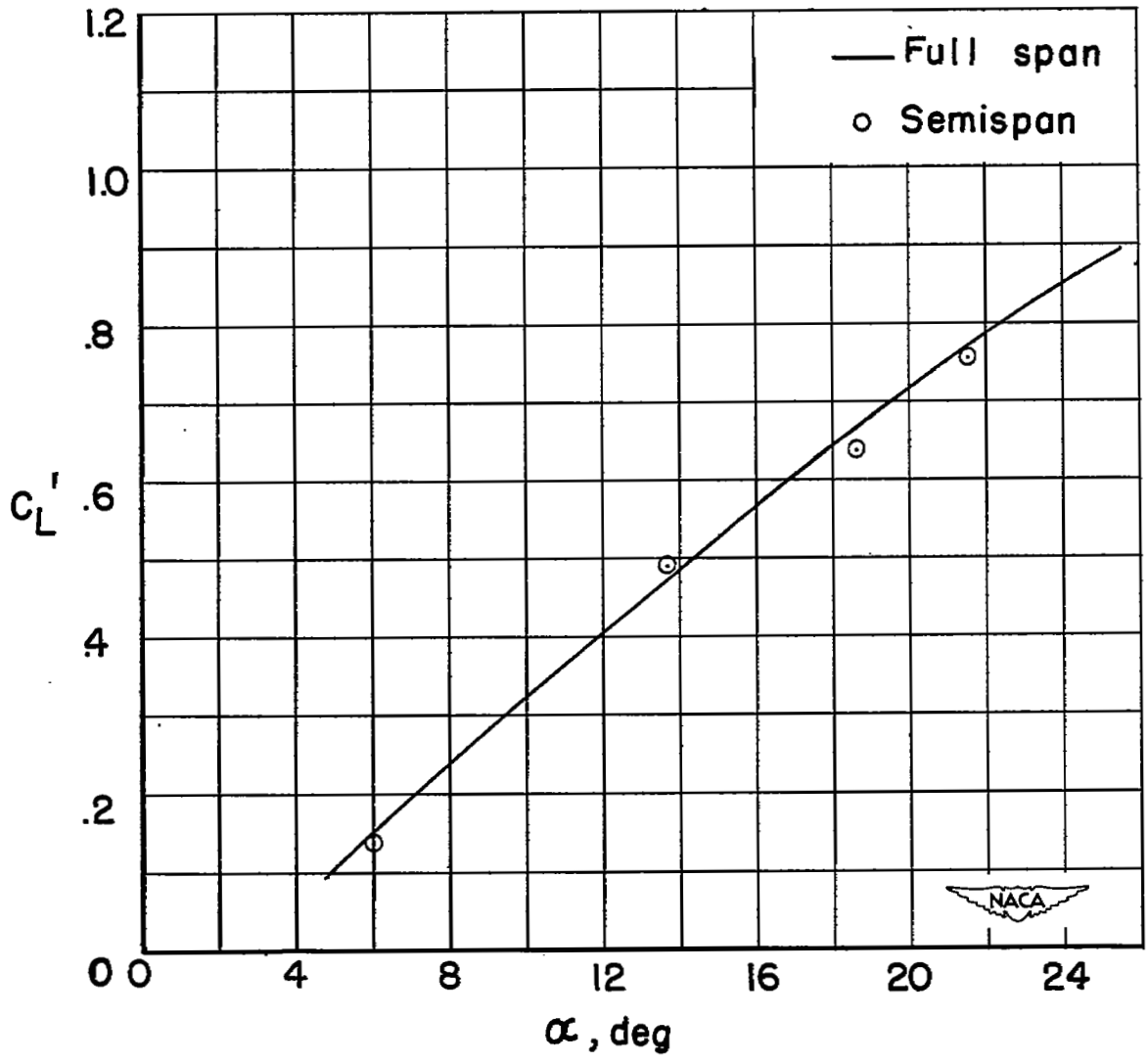

Figure 16.- Variation of wing lift coefficient with angle of attack. Wing with 1.00b/2 drooped-nose flap deflected 40°.

[redacted]

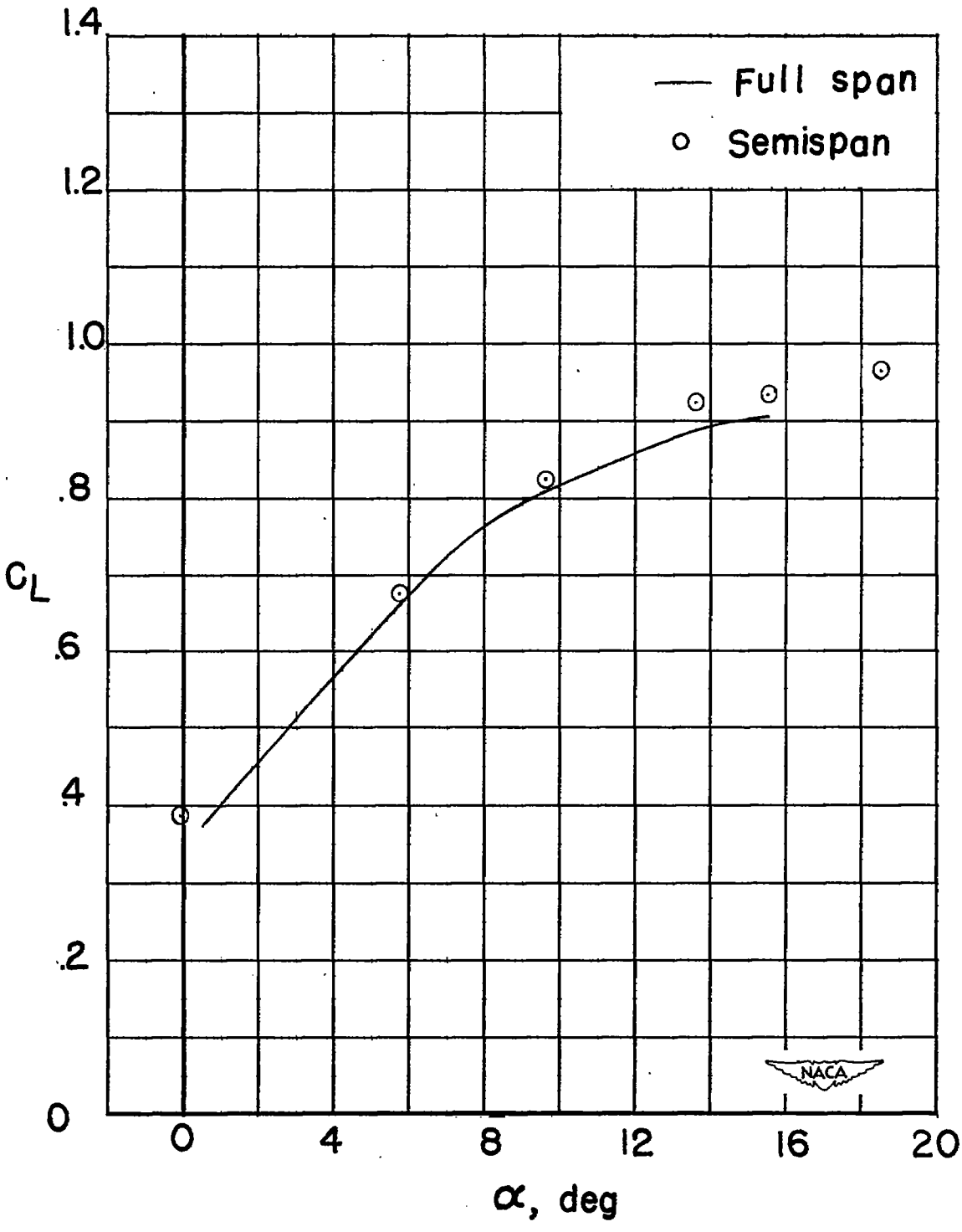

Figure 17.- Variation of wing lift coefficient with angle of attack. Wing with 0.50b/2 trailing-edge flap deflected 40°.

[redacted]

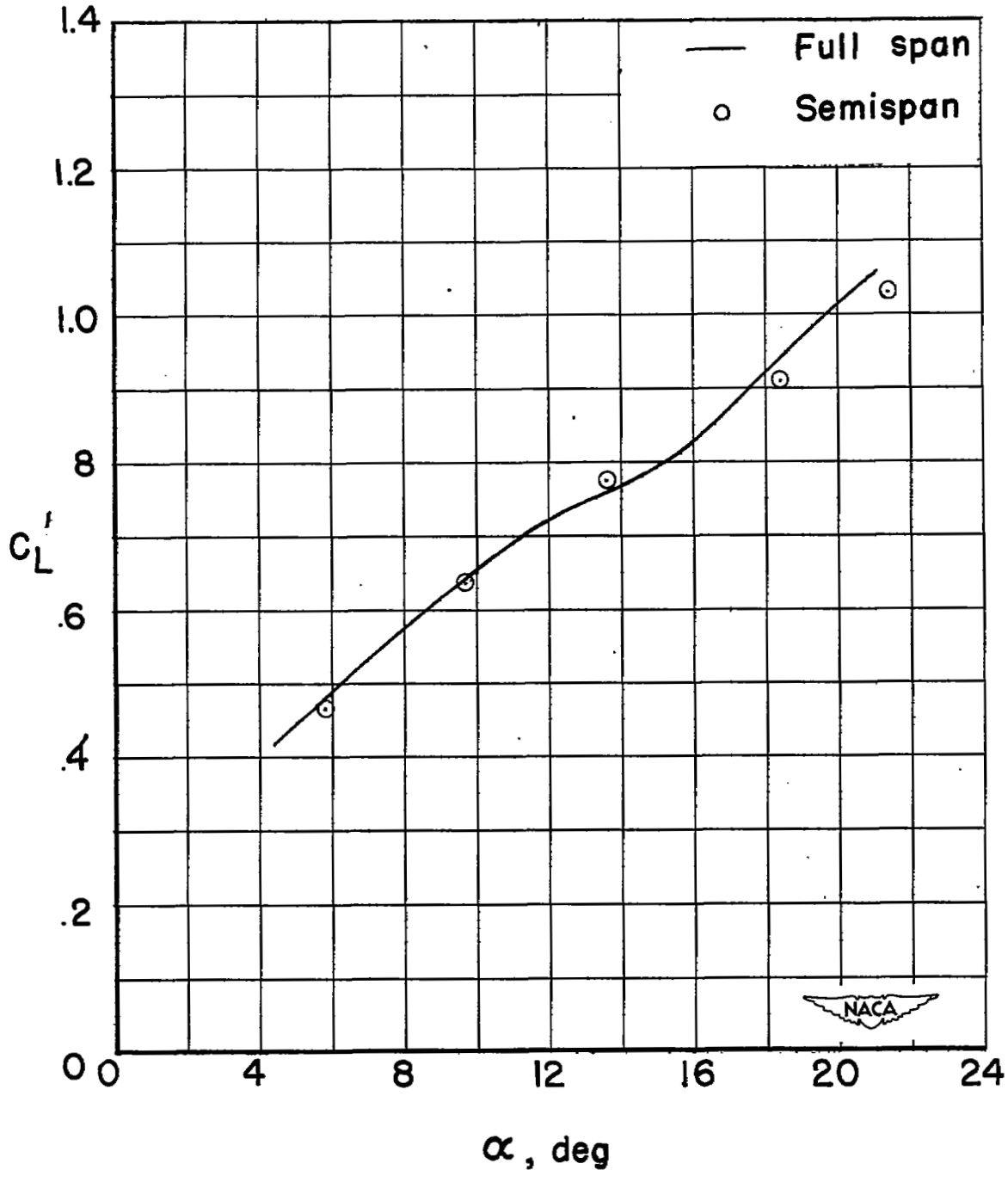

Figure 18.- Variation of wing lift coefficient with angle of attack. Wing with 0.50b/2 trailing-edge flap and 1.00b/2 drooped-nose flap deflected 40°.

[redacted]

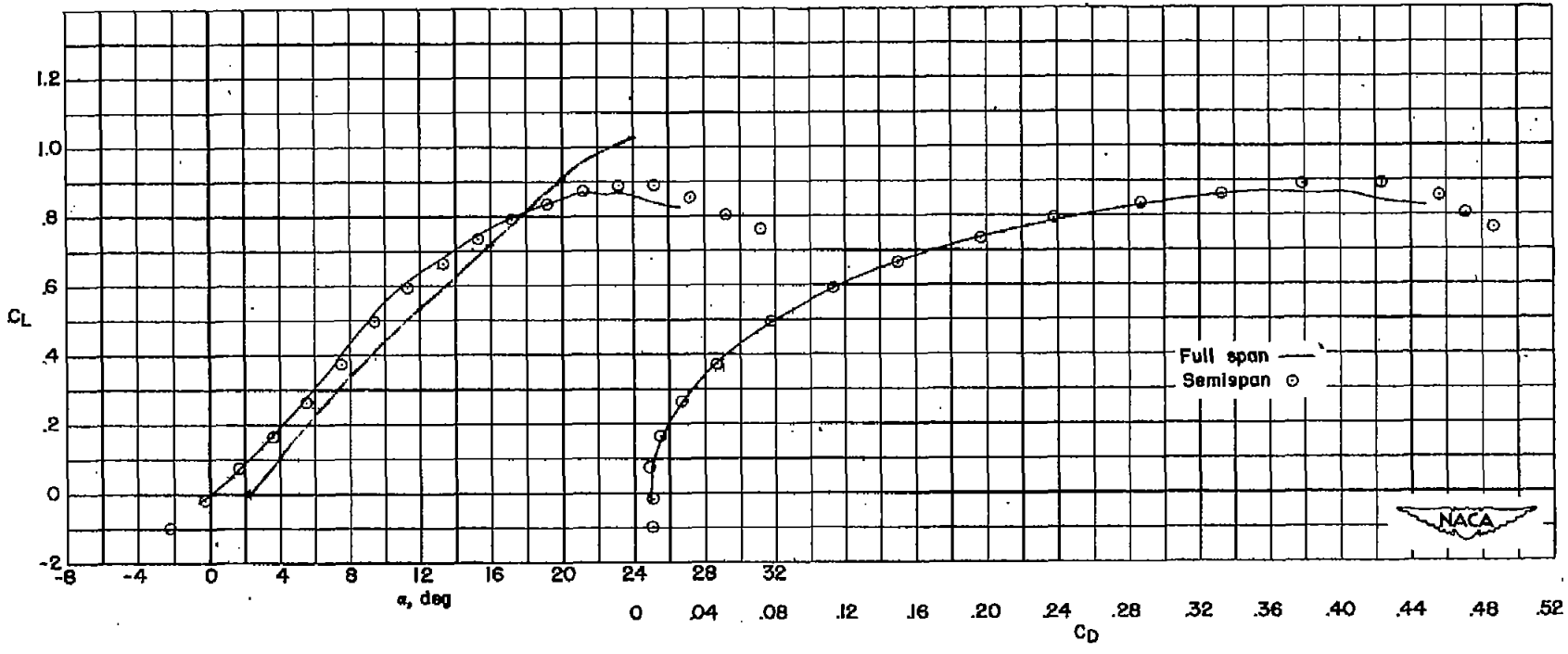

(a) Basic wing.

Figure 19.- Lift and drag characteristics for four flapped configurations of the full-span and semispan 47.5° sweptback wing.

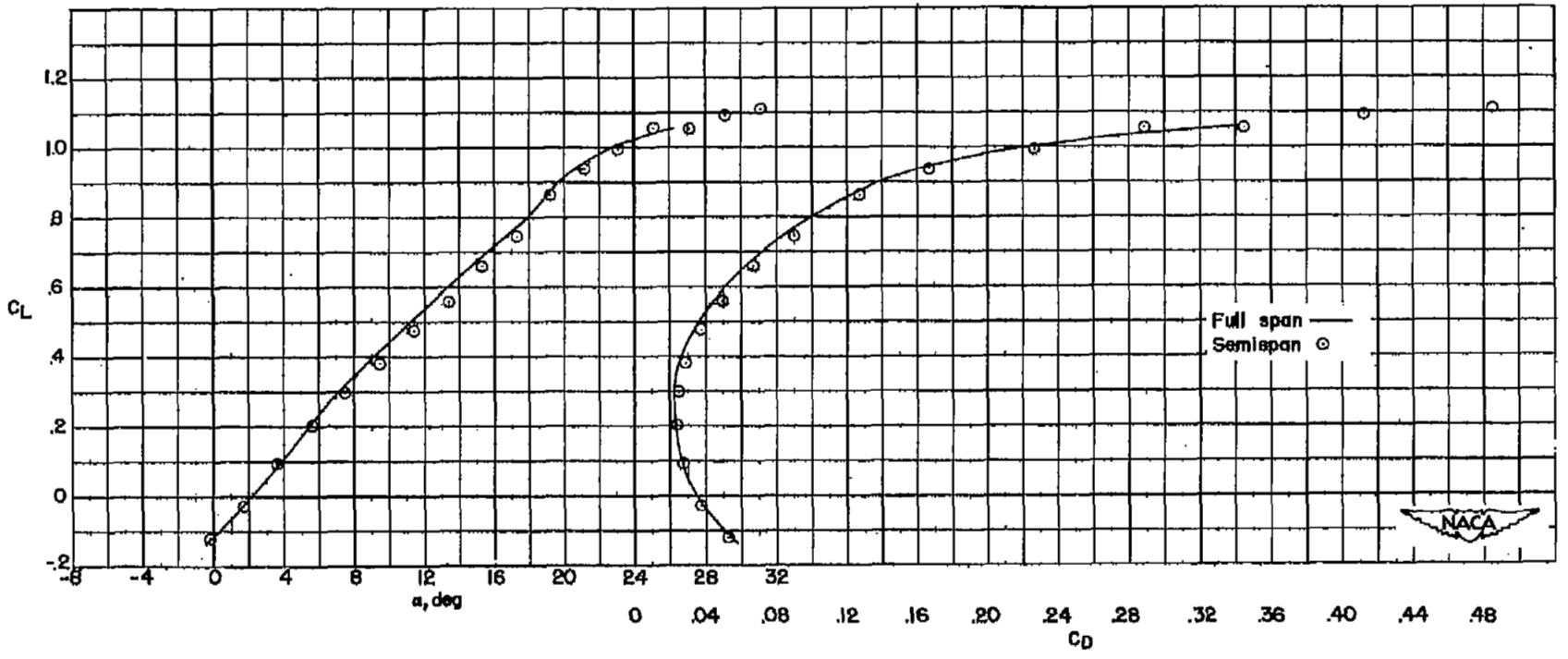

(b) Wing with 1.00b/2 drooped-nose flap deflected 30°.

Figure 19.- Continued.

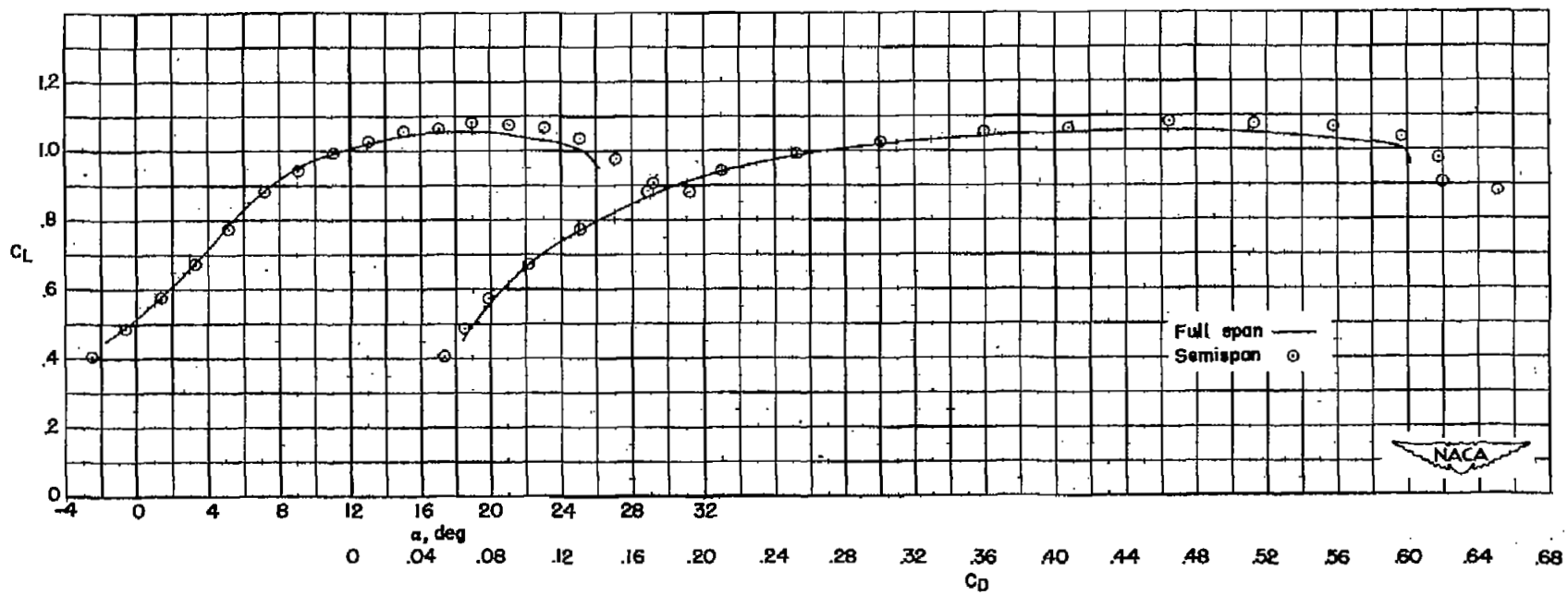

(c) Wing with 1.00b/2 trailing-edge flap deflected 40°.

Figure 19.- Continued.

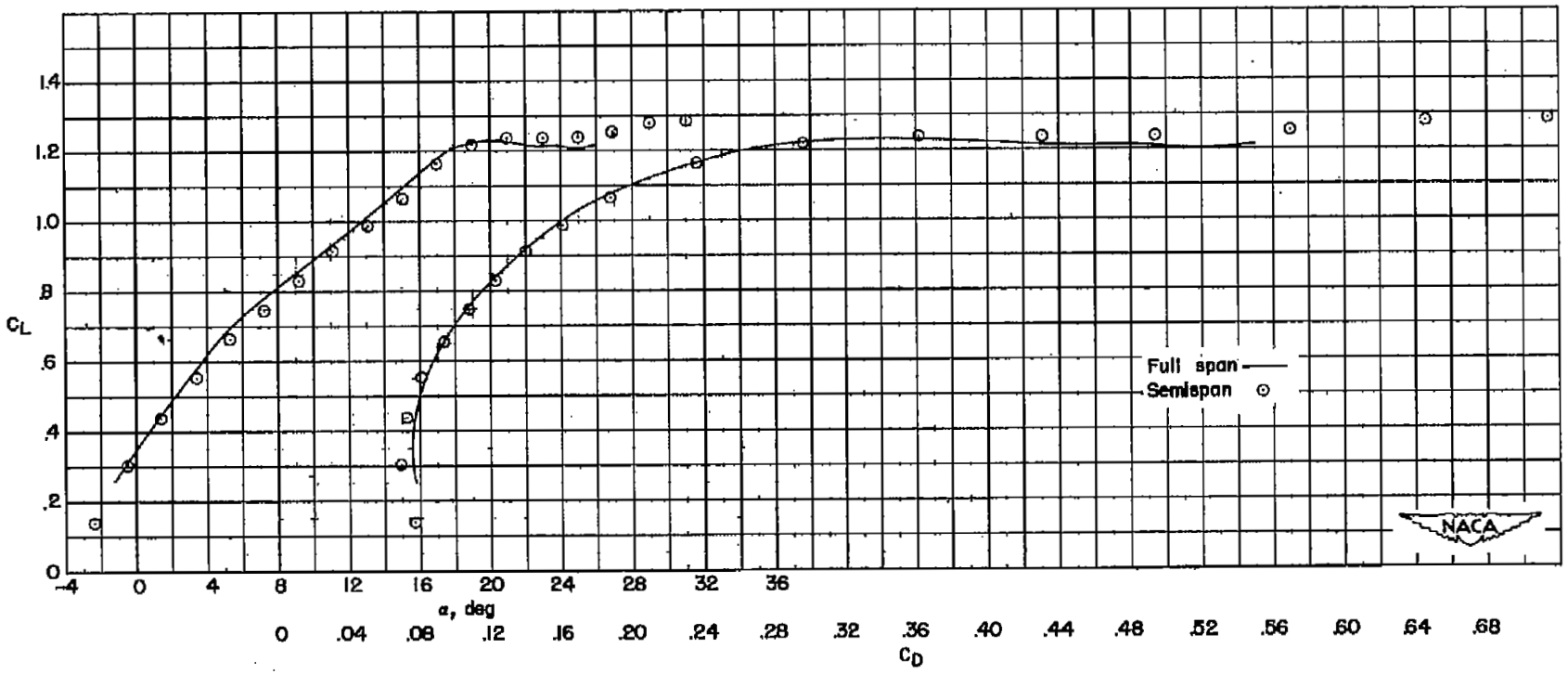

(d) Wing with 1.00b/2 drooped-nose flap deflected 30° plus 1.00b/2 trailing-edge flap deflected 40°.

Figure 19.- Concluded.

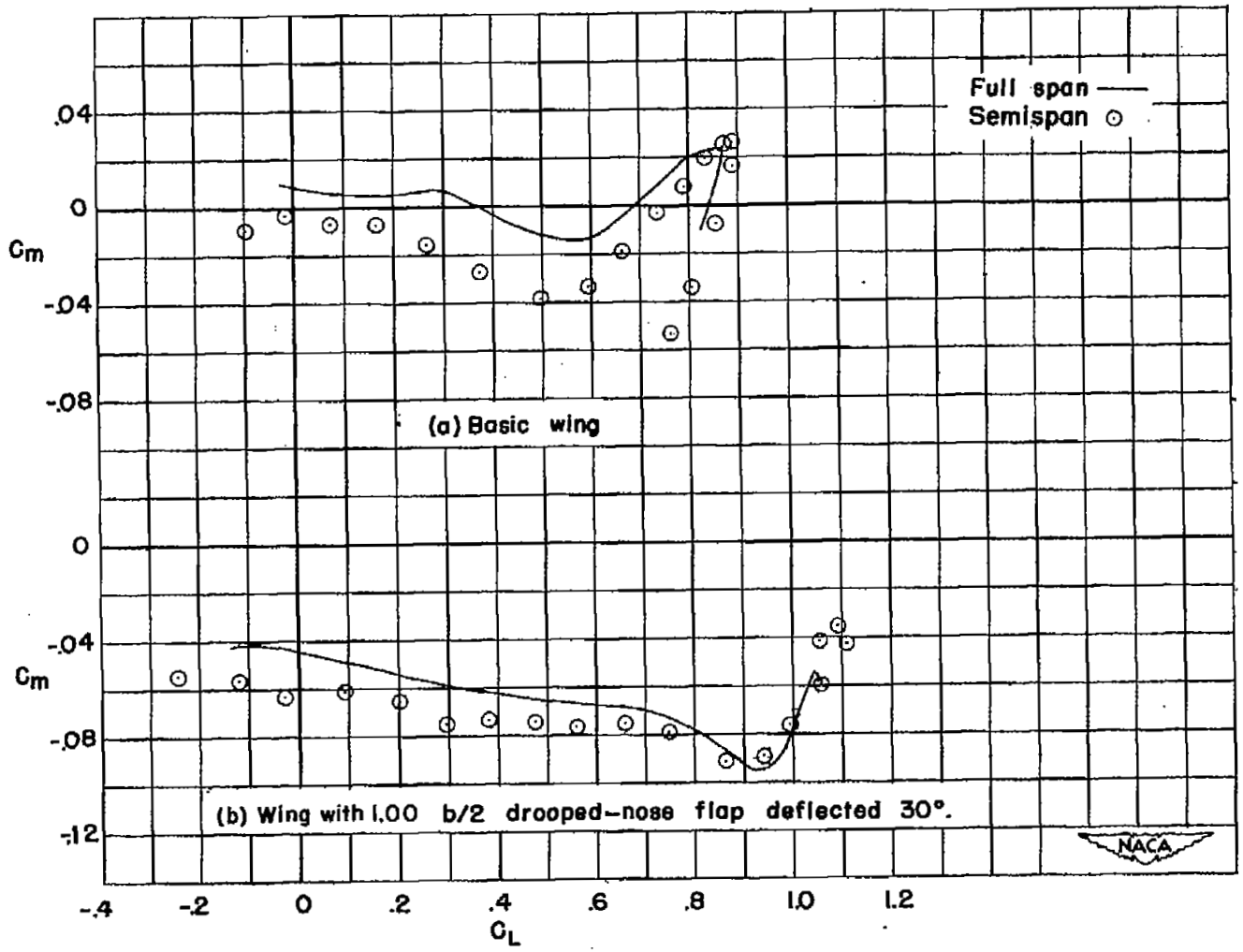

Figure 20.- Pitching-moment characteristics for four flapped configurations of the full-span and semispan 47.5° swept-back wing.

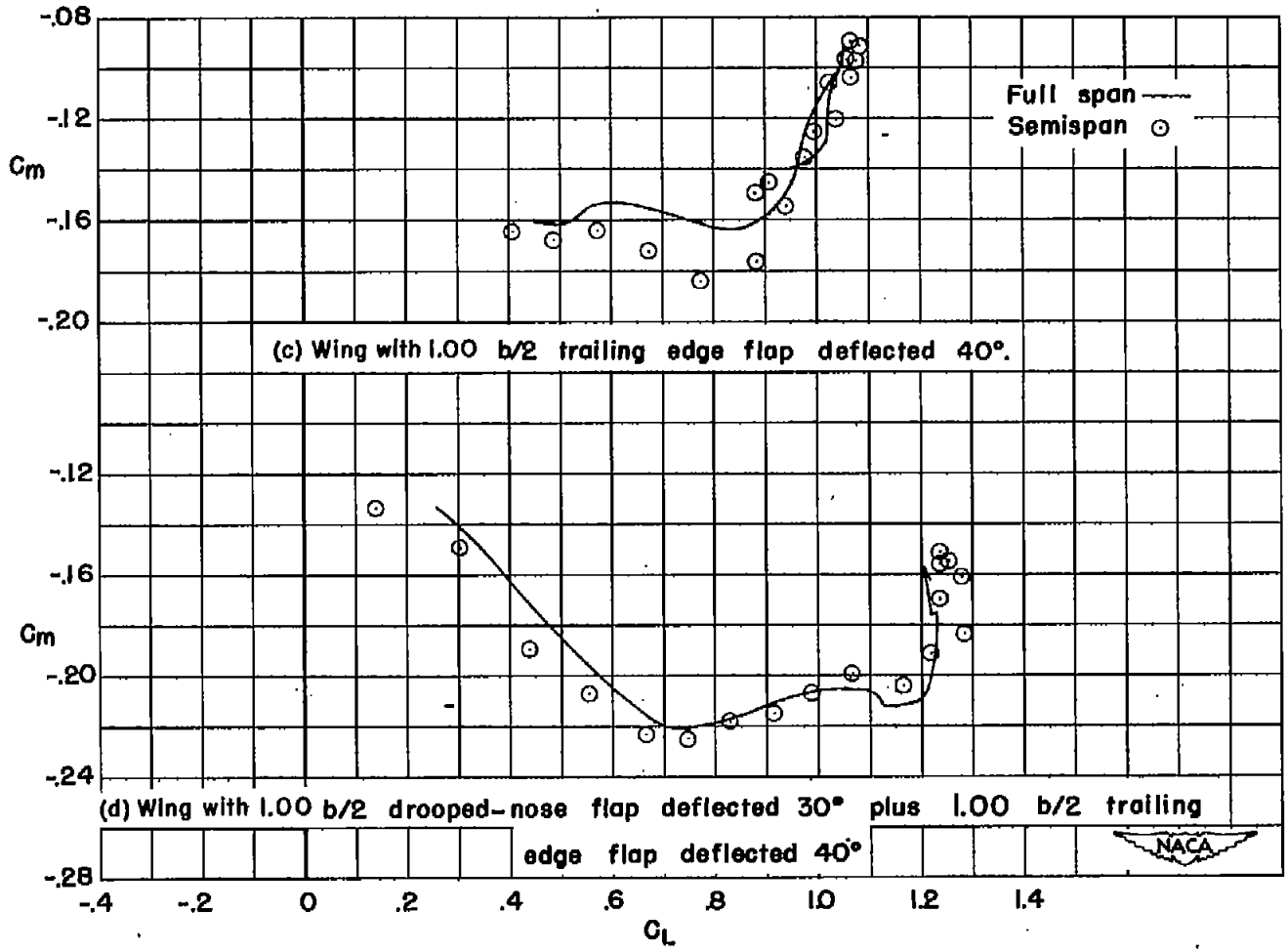

Figure 20.- Concluded.

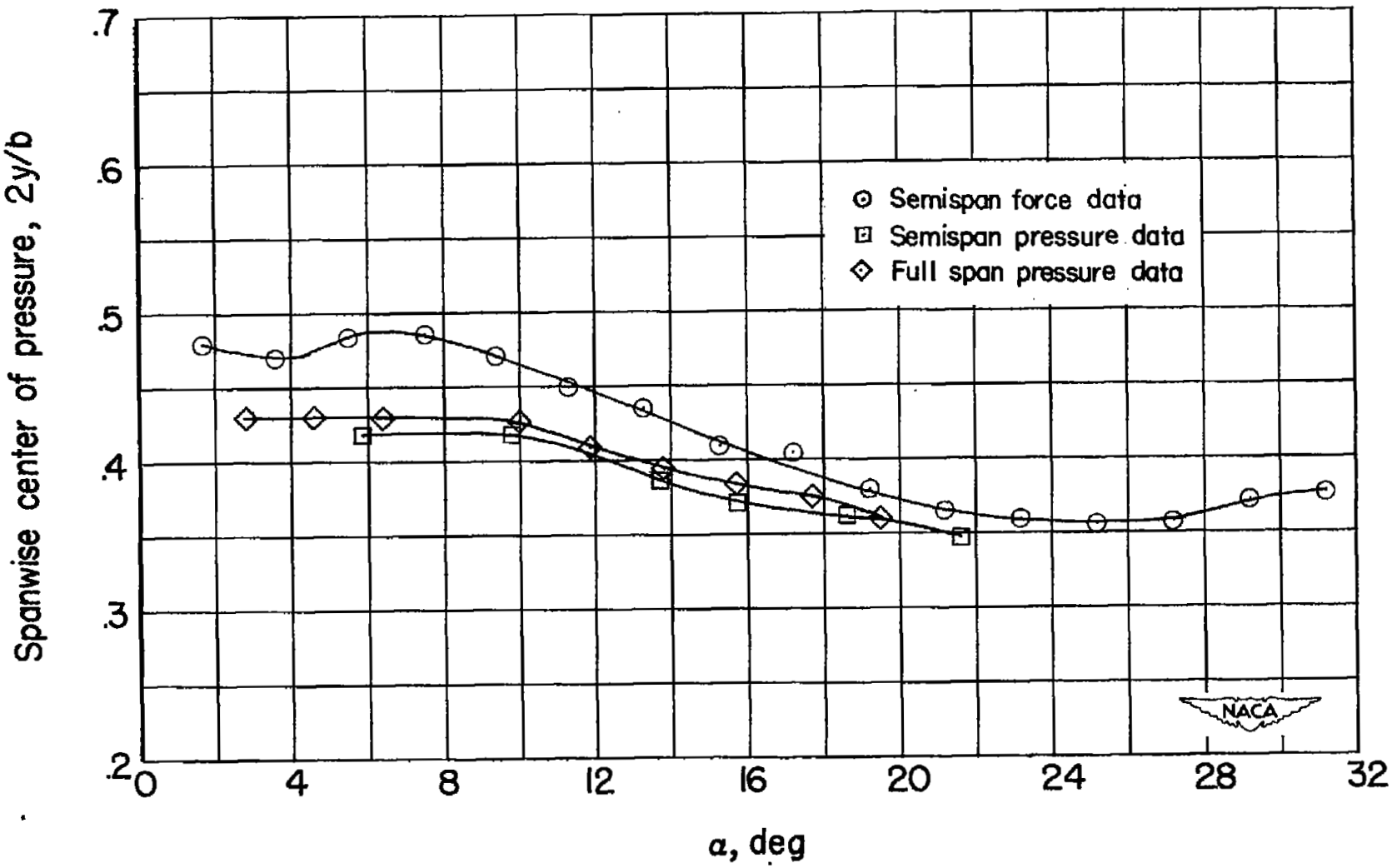

Figure 21.- Variation of spanwise location of wing center of pressure with angle of attack. Basic wing.

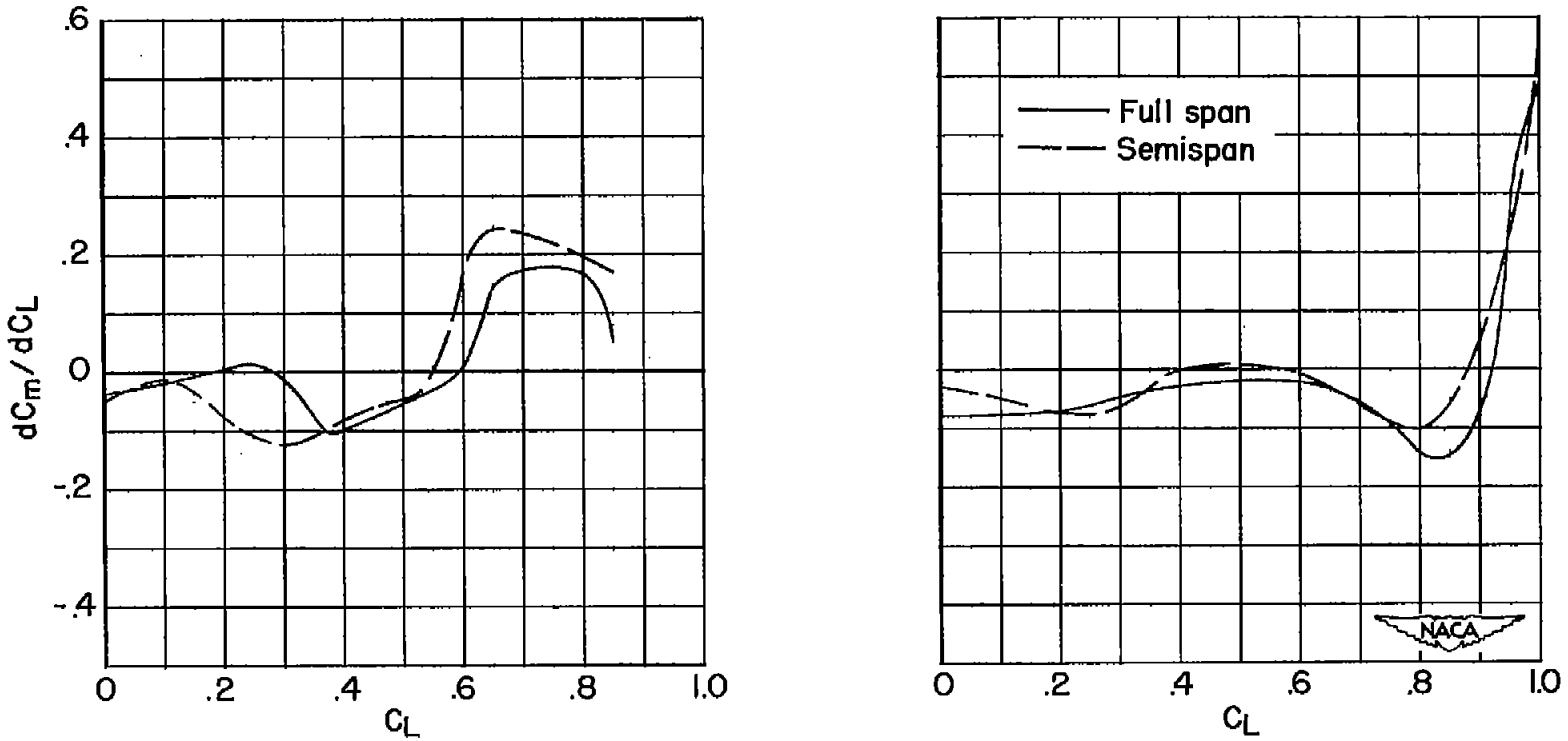

(a) Basic wing.

(b) Wing with 1.00b/2 drooped-nose flap deflected 30°.

Figure 22.- Variation of dC_m/dC_L with C_L for four flapped configurations of the full-span and semispan 47.5° sweptback wing.

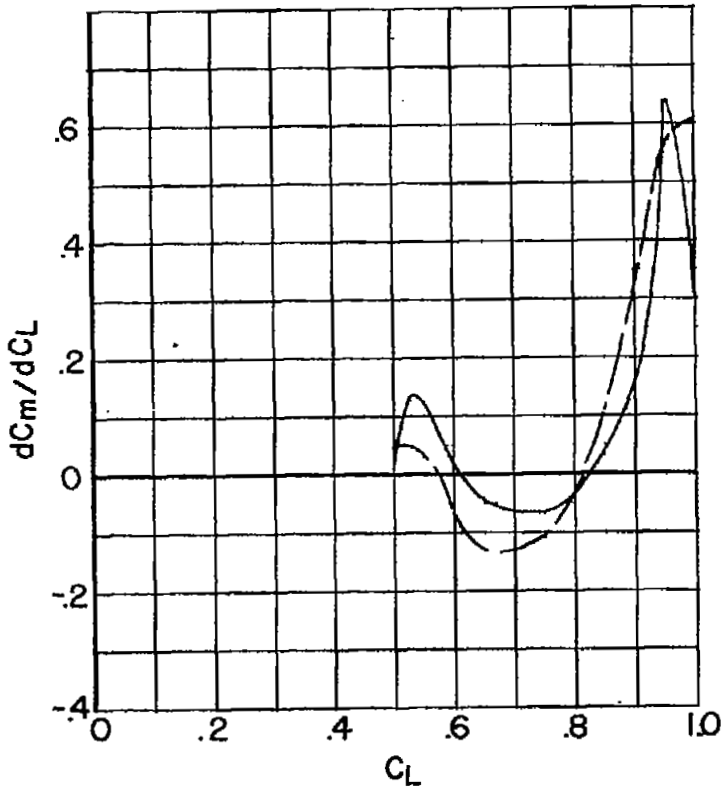

(c) Wing with 1.00b/2 trailing-edge flap deflected 40°.

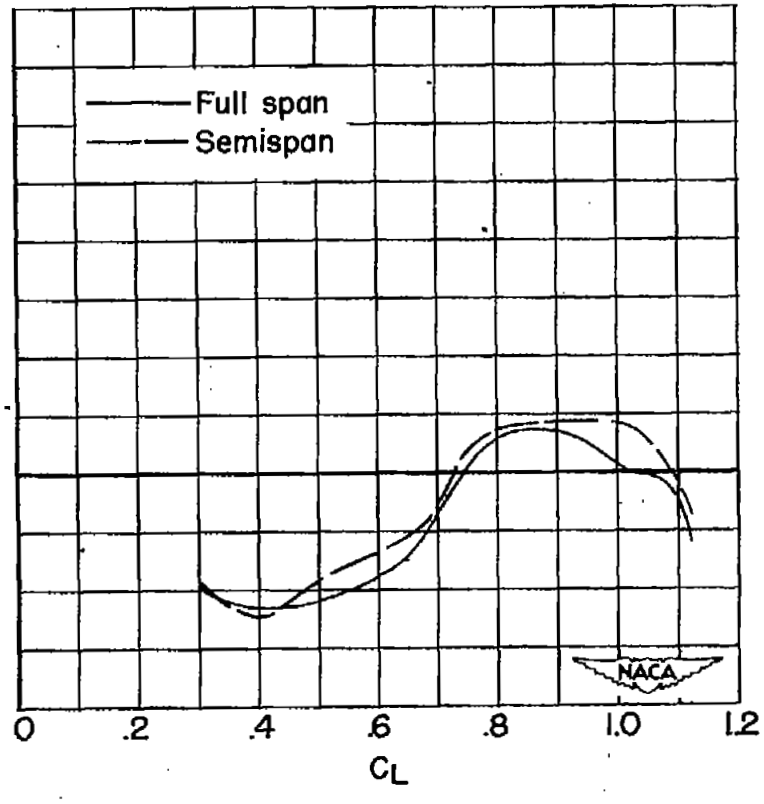

(d) Wing with 1.00 drooped-nose flap deflected 30° plus 1.00b/2 trailing-edge flap deflected 40°.

Figure 22.- Concluded.

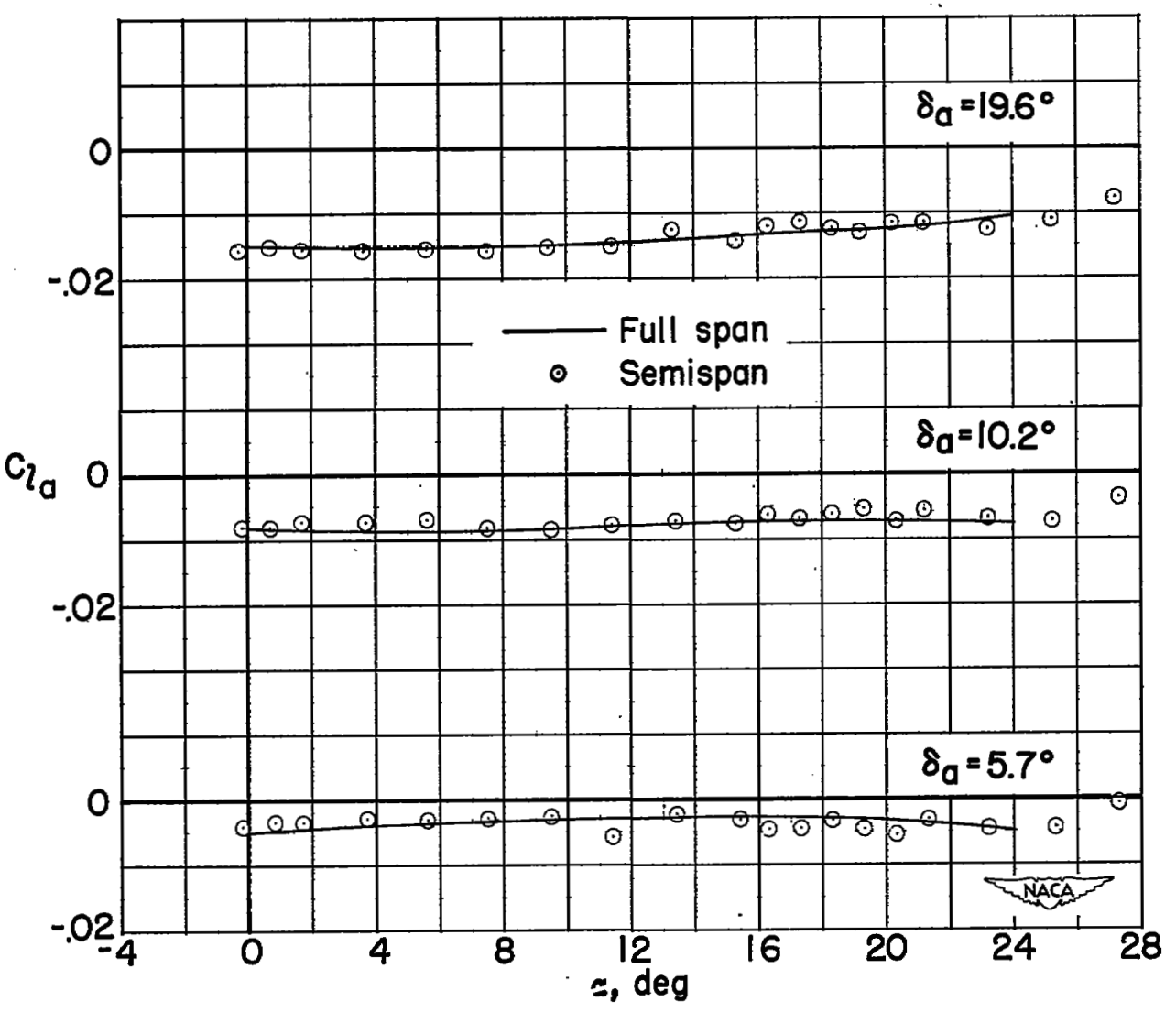

Figure 23.- Rolling-moment characteristics due to aileron deflection for the full-span and semispan 47.5° sweptback wing.

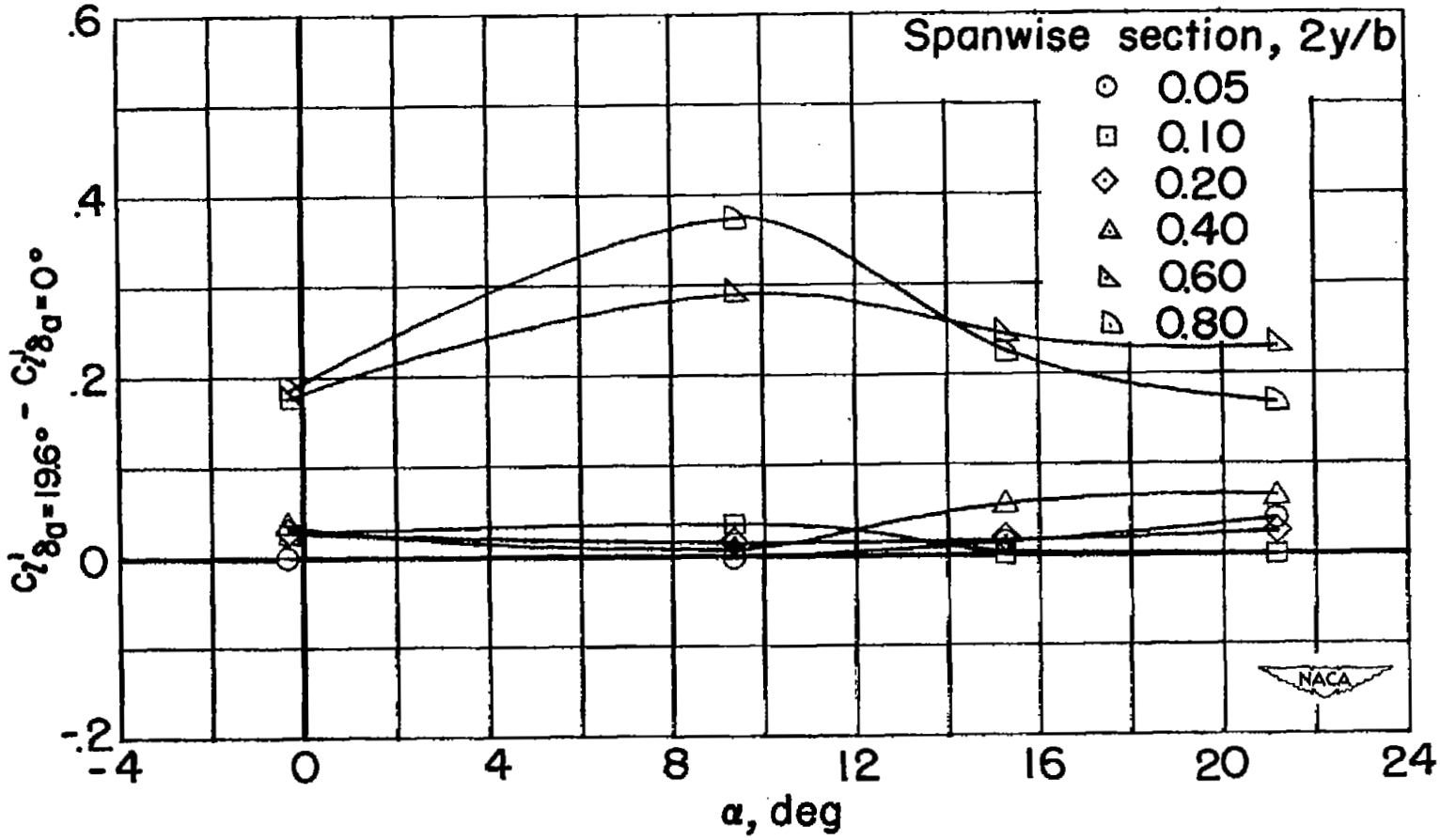

Figure 24.- Effect of 19.6° aileron deflection on section lift characteristics of semispan 47.5° sweptback wing.

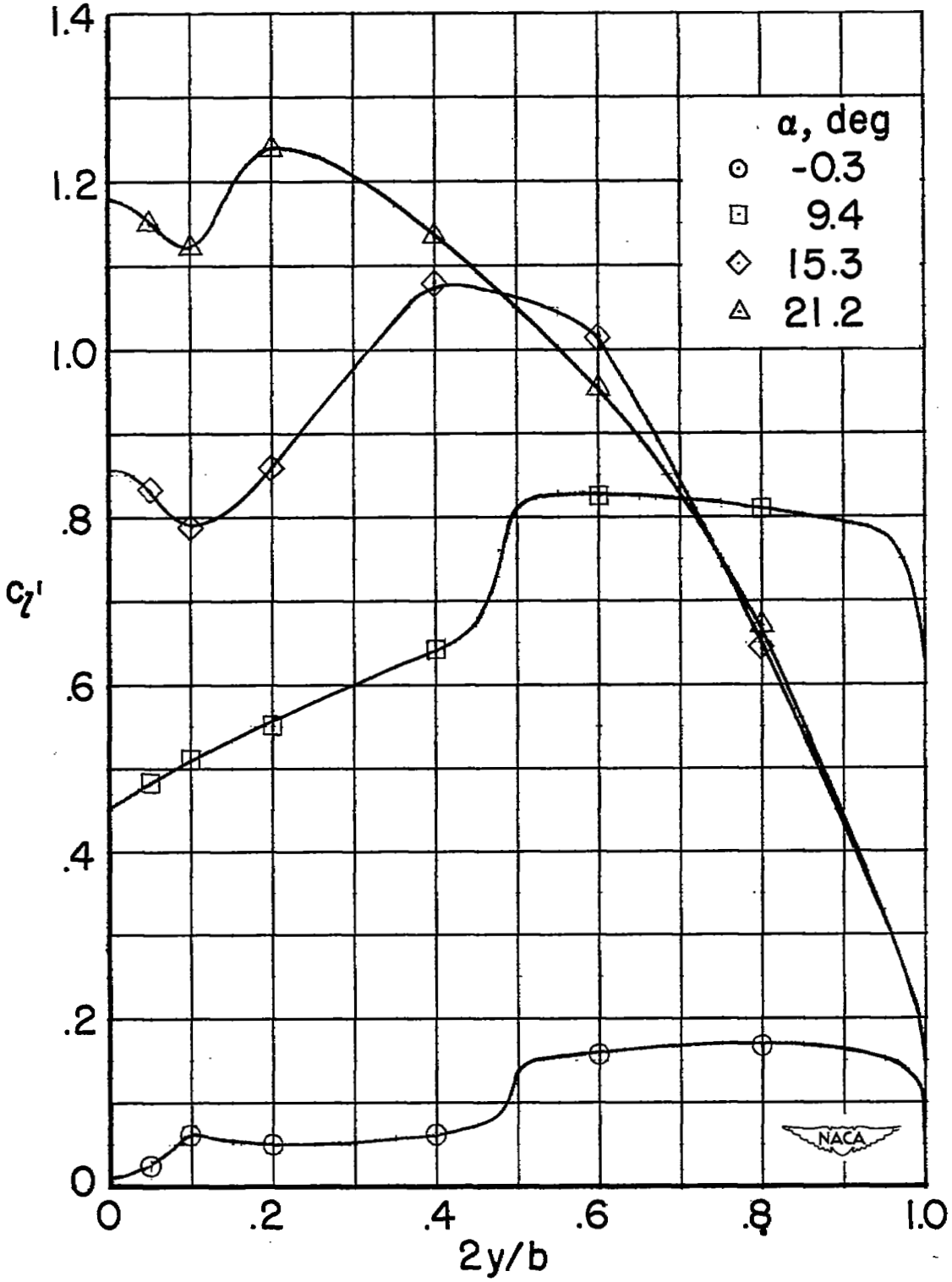

Figure 25.- Span loading characteristics of the semispan 47.5° sweptback wing with a 19.6° aileron deflection.

[redacted]

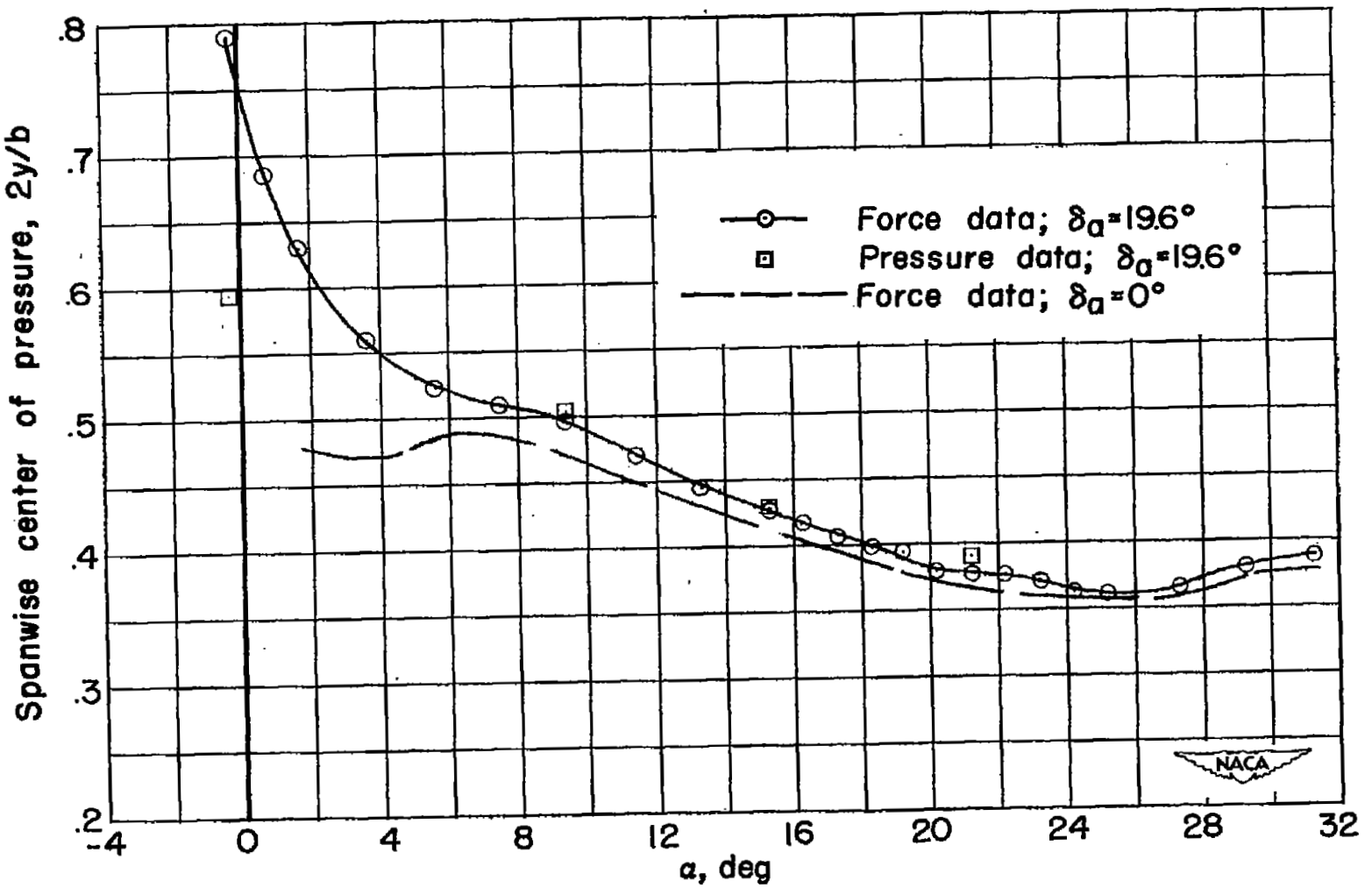

Figure 26.- Variation of spanwise location of wing center of pressure with angle of attack for the semispan 47.5° sweptback wing with a 19.6° aileron deflection.

NACA-Langley - 12-6-51 - 325